nature communications

Article

https://doi.org/10.1038/s41467-024-54344-5

The nutrient-sensing Rag-GTPase complex in B cells controls humoral immunity via TFEB/TFE3-dependent mitochondrial fitness

Received: 22 March 2024

Accepted: 5 November 2024

Published online: 23 November 2024

Check for updates

Xingxing Zhu[1], Yue Wu[2,3], Yanfeng Li[1], Xian Zhou[1], Jens O. Watzlawik[4], Yin Maggie Chen[5], Ariel L. Raybuck[6], Daniel D. Billadeau[5], Virginia Smith Shapiro[5], Wolfdieter Springer[4,7], Jie Sun[2,3], Mark R. Boothby[6] & Hu Zeng[1,5]

Germinal center (GC) formation, which is an integrant part of humoral immunity, involves energy-consuming metabolic reprogramming. Rag-GTPases are known to signal amino acid availability to cellular pathways that regulate nutrient distribution such as the mechanistic target of rapamycin complex 1 (mTORC1) pathway and the transcription factors TFEB and TFE3. However, the contribution of these factors to humoral immunity remains undefined. Here, we show that B cell-intrinsic Rag-GTPases are critical for the development and activation of B cells. RagA/RagB deficient B cells fail to form GCs, produce antibodies, and to generate plasmablasts during both T-dependent (TD) and T-independent (TI) humoral immune responses. Deletion of RagA/RagB in GC B cells leads to abnormal dark zone (DZ) to light zone (LZ) ratio and reduced affinity maturation. Mechanistically, the Rag-GTPase complex constrains TFEB/TFE3 activity to prevent mitophagy dysregulation and maintain mitochondrial fitness in B cells, which are independent of canonical mTORC1 activation. TFEB/TFE3 deletion restores B cell development, GC formation in Peyer's patches and TI humoral immunity, but not TD humoral immunity in the absence of Rag-GTPases. Collectively, our data establish the Rag GTPase-TFEB/TFE3 pathway as a likely mTORC1 independent mechanism to coordinating nutrient sensing and mitochondrial metabolism in B cells.

During infection or immunization, B lymphocytes can be activated in a T cell-dependent (TD) or -independent (TI) manner, differentiate into plasmablast cells or form germinal center (GC) and subsequently differentiate into memory B cells and plasma cells[1–4], which produce different isotypes of antibodies[5]. There is increasing evidence that metabolic programming underpins B cell development, quiescence, activation, and differentiation[6–8]. Specifically, glucose metabolism is vital to support the B cell function like early B cell development in bone marrow (BM), affinity maturation of GC B cells, and lymphomagenesis[9–11]. Lactate dehydrogenase-dependent glycolysis is dispensable for TI responses, but critical for TD responses, highlighting divergent metabolic requirements between TD and TI

[1]Division of Rheumatology, Department of Medicine, Mayo Clinic Rochester, Rochester, MN, USA. [2]Carter Immunology Center, University of Virginia, Charlottesville, VA, USA. [3]Division of Infectious Diseases and International Health, Department of Medicine, University of Virginia, Charlottesville, VA, USA. [4]Department of Neuroscience, Mayo Clinic, Jacksonville, FL, USA. [5]Department of Immunology, Mayo Clinic Rochester, Rochester, MN, USA. [6]Department of Pathology, Microbiology & Immunology, Molecular Pathogenesis Division, Vanderbilt University Medical Center and School of Medicine, Nashville, TN, USA. [7]Neuroscience PhD Program, Mayo Clinic Graduate School of Biomedical Sciences, Jacksonville, FL, USA. e-mail: Zeng.hu1@mayo.edu

responses[10]. Mitochondria oxidative phosphorylation, amplified by CD40L or Toll-like receptor (TLR) ligand engagement, supports B cell survival and differentiation[12–15]. Nutrients modulate cellular metabolic reprogramming and subsequently affect immune responses[16–18]. Consequently, malnutrition, including Kwashiorkor, a form of severe protein inadequacy, is associated with small Peyer's patches (PP) and GC, fewer antibody-producing cells, and increased susceptibility to infection[19,20]. A potential mechanism through which amino acid controls immunity is the tuning of mTORC1 activation[16]. Yet, how B cells sense nutrients to coordinate their mitochondrial metabolism, and how metabolic pathways support B cell development and responses to TD and TI antigens, remains poorly defined.

Rag-GTPases are the key amino acid sensors that relay amino acid availability to modulate mTORC1 and suppress TFEB transcription factor[21–23]. As small GTPases, Rags are obligate heterodimers, configured such that RagA or RagB is bound to RagC or RagD. RagA is required for amino acid-dependent mTORC1 activation in vitro[21,23]. Gain of function mutations in Rag-GTPases leads to overactivation of mTORC1 in B cells, demonstrating that Rag-GTPases are sufficient for mTORC1 activation[24,25]. Yet, there is controversy regarding the necessity of Rag-GTPases for activation of canonical mTORC1[26–30]. In fact, Rag-GTPases can even suppress mTORC1 signaling because RagA/RagB deficient macrophages exhibit highly elevated mTORC1 activity, indicating a cell type-specific, context-dependent relationship between Rag-GTPases and mTORC1[31]. Recent studies have demonstrated that Rag-GTPases cooperate with Rheb to activate mTORC1 to support Treg functions[32–34]. However, the mechanisms through which Rag-GTPases coordinate mTORC1 and TFEB to regulate humoral immunity are currently unknown.

MiTF/TFE family members, including MITF, TFEB, TFE3, and TFEC, are basic helix-loop-helix leucine zipper (bHLH-Zip) transcription factors. They share a similar structure and often express together[35]. Among them, TFEB and TFE3 regulate a similar set of genes involved in lysosomal biogenesis, lipid metabolism, autophagy, and stress response[36–38]. They can undergo cytoplasm-to-nucleus shuttling in response to different nutrition statuses, which is governed by the phosphorylation through kinases such as mTORC1, ERK, and GSK3[39–42]. TFEB/TFE3 can promote autophagy and production of proinflammatory cytokines in macrophages in vitro, but it can also enhance mTORC1 activation in tumor-associated macrophages[31,43,44]. In adaptive immunity, TFEB/TFE3 supports CD40 ligand expression on T cells, maintains regulatory T cell functions, and may prevent B cell senescence during aging[45–47]. Their B cell-intrinsic functions in cellular metabolism and humoral immune response have not been explored.

Here, we take a genetic approach to dissect the contributions of Rag-GTPases and mTORC1 to B cell development and function in vivo. Our study shows that B cell-intrinsic Rag-GTPases are essential for B cell development, GC formation in PPs, dark zone (DZ) and light zone (LZ) distribution in GC, TD, and TI antigen immunization-induced antibody responses, but largely dispensable for mTORC1 activity. Mechanistically, Rag-GTPase mediates inhibition of TFEB/TFE3 activity and prevention of abnormal mitophagy are required for optimal B cell activation, mitochondrial metabolism, humoral immunity towards TI, but not TD, antigen immunization, and GC formation in PPs. Collectively, our results demonstrate that the amino acid sensing complex Rag-GTPases maintains mitochondrial fitness by suppressing TFEB/TFE3 activity in B cells to support the humoral immune responses, in a likely mTORC1-independent manner.

Results

Amino acids modulate mTORC1 independent of Rag-GTPases

Amino acids (AAs) are the key nutrients engaging Rag-GTPases and mTORC1 signaling[40]. To evaluate the impact of AAs on B cell activation and mTORC1 activity, we stimulated B cells in full AAs, essential AAs (EAA) or no AA condition. Among the three conditions, full AA-induced the largest cell size, highest expression of CD86, amino acid transporter CD98, and phosphorylation of ribosomal protein S6 (p-S6) and eukaryotic initiation factor 4E-binding protein 1 (p-4EBP1), markers for mTORC1 activation, while B cells in no AA condition had the lowest expression of these markers (Fig. 1A). When we activated B cells in the presence of a titrated concentration of AAs, we observed that AAs promote B activation in a concentration-dependent manner (Fig. 1B). Taken together, these data suggest that AAs can fine-tune B cell activation and mTORC1 activity.

Given the contention regarding the link between Rag-GTPases and mTORC1[26–30], we directly compared the phenotypes between Rag-GTPase deficiency and mTORC1 deficiency in B cells. RagA and RagB or Raptor were acutely deleted by tamoxifen injection into $Cre^{ER}Rraga^{fl/fl}Rragb^{fl/fl}$ mice or $Cre^{ER}Rptor^{fl/fl}$ mice (Supplementary Fig. 1A, B), which did not significantly alter mature B cell compartment in spleens, including follicular B cells and marginal zone B cells (Supplementary Fig. 1C, D). Raptor deficient splenic B cells had diminished p-S6 and p-4EBP1 levels, reduced CD98 expression and cell size in either full AA medium or no AA medium (Fig. 1C). In contrast, RagA/RagB deficient B cells did not exhibit reduction of any of these parameters in full AA medium. However, under no AA condition, all these parameters reduced to a largely comparable level between 3 genotypes (Fig. 1C), suggesting a Rag-GTPase independent but AA dependent regulation of mTORC1 and initial B cell activation. Immunoblot analysis on B cells activated in full AA medium at different time points confirmed that Raptor deficiency nearly abolished p-4EBP1, p-S6K and p-S6 (Fig. 1D and Supplementary Fig. 1E), which were largely intact in the absence of RagA/RagB at early timepoint of activation (Fig. 1D). Still, RagA/RagB deficient B cells had modestly (and variably) reduced p-S6 and intact p-4EBP1 at late timepoint (72 h) of activation (Supplementary Fig. 1F). Consistent with previous publications[16,48], Raptor deficient B cells exhibited substantially reduced proliferation upon various antigenic stimulations. In contrast, RagA/RagB deletion did not affect the proliferation or apoptosis of B cells (Fig. 1E and Supplementary Fig. 1G). However, the class switch to IgG1-producing B cells induced by LPS was reduced in both Rag-GTPases or Raptor deficient B cells (Fig. 1F), suggesting a proliferation-independent class switch defect in RagA/RagB deficient B cells. Furthermore, rapamycin treatment exacerbated the IgG1 expression defect in RagA/RagB deficient B cells in a dose-dependent manner, suggesting nonredundant roles between mTORC1 and Rag-GTPase during B cell activation (Fig. 1G). Consistent with the reduced IgG1 expression, both Raptor and RagA/RagB deficient B cells showed reduced activation-induced cytidine deaminase (AID) induction (Fig. 1D). Thus, amino acids modulate mTORC1 independent of Rag-GTPases. Rag-GTPases can regulate B cell class switching likely independent of canonical mTORC1 activity in vitro.

Acute deletion of Rag-GTPases blocks early B cell development and abolishes germinal center B cells in Peyer's patches

Constitutive deletion of Raptor blocks early B cell development at pro-B to pre-B transition[8,49]. While acute deletion of Raptor or RagA/RagB did not affect mature B cells in spleens, we examined the potential impacts on early B cell development. Tamoxifen-injected $Cre^{ER}Rraga^{fl/fl}Rragb^{fl/fl}$ mice had relatively normal frequencies but reduced absolute numbers of $B220^{+}CD43^{+}IgM^{-}$ B cell precursors, which were largely intact in tamoxifen-injected $Cre^{ER}Rptor^{fl/fl}$ mice (Fig. 2A-B). Later stage B cells, including $B220^{lo}CD43^{-}$ pre-B cells/immature B cells and $B220^{hi}CD43^{-}$ circulating mature B cells, were mostly reduced in the absence of RagA/RagB (Fig. 2A). In contrast, Raptor deficiency significantly reduced pre-B cells/immature B cells, but increased circulating mature B cells (Fig. 2B). The contrasting circulating mature B cell phenotypes were associated with altered expression of CXCR4, a key chemokine receptor regulating B cell retention in bone marrow[50], which increased in the absence of Raptor, but reduced in the absence of RagA/RagB (Supplementary Fig. 1H). Within B cell precursors, the

https://doi.org/10.1038/s41467-024-54344-5

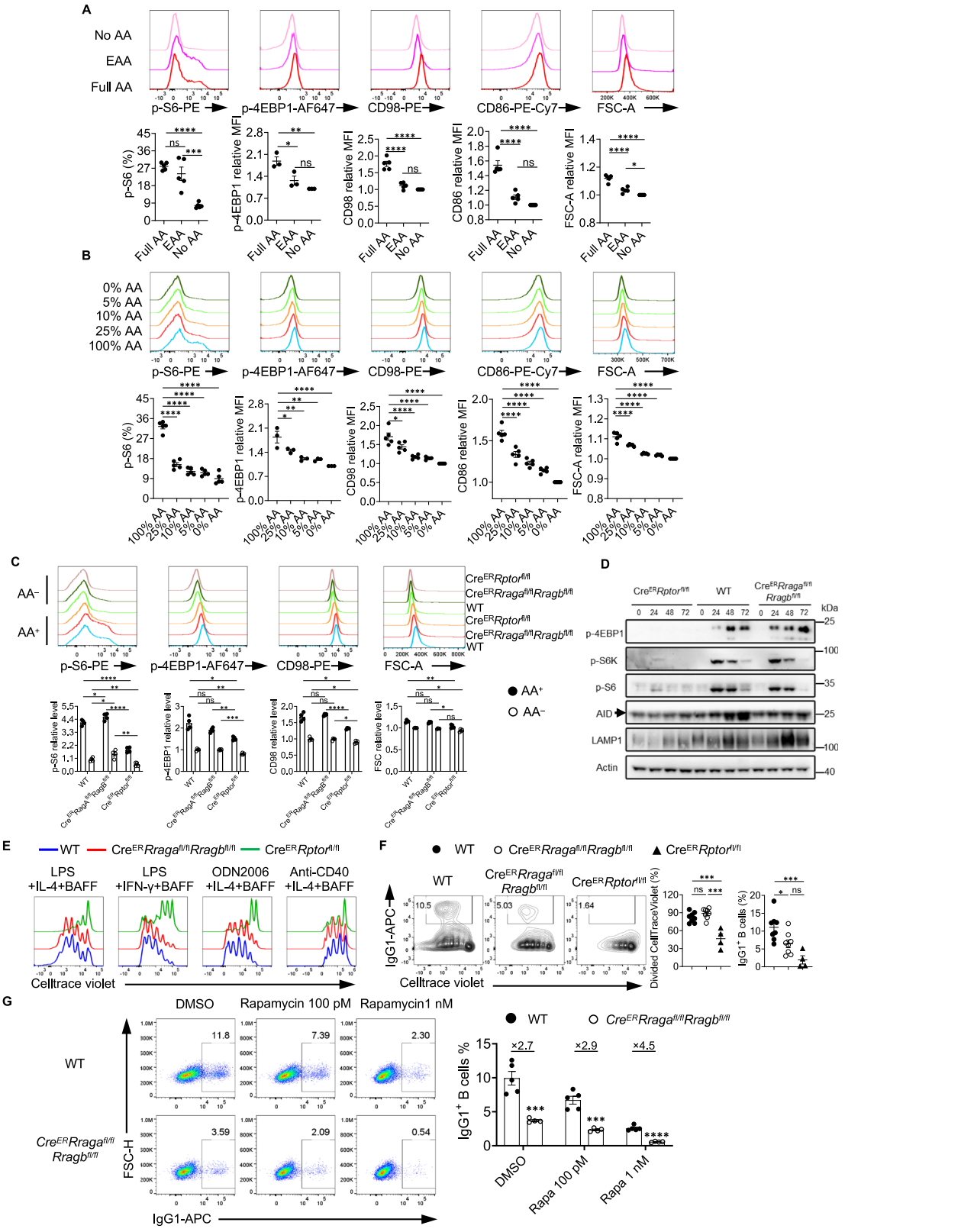

frequencies of fraction B and fraction C/C′ were significantly reduced in the absence of either Rag-GTPases or mTORC1 (Fig. 2C, D). These data indicate that acute loss of either Rag-GTPases or mTORC1 reduces frequencies of fraction B and fraction C/C′ precursors. We did not observe any developmental defects in Cre^{ER}*Rragb*$^{fl/fl}$ mice (Supplementary Fig. 1I, J). Thus, both Rag-GTPases and mTORC1 are critically required for early B cell development, but they may have different functions in the maintenance or retention of B220^{+}CD43^{+}IgM^{-} B cell precursors and circulating mature B cells. In addition, RagA and RagB have redundant functions in B cell development.

Acute deletion of either Rag-GTPases or mTORC1 preserves naïve mature CD4^{+} T and B cells in spleens (Supplementary Fig. 1C, D). However, we found that the frequencies and absolute numbers of GC B cells significantly decreased in PPs of both Cre^{ER}*Rraga*$^{fl/fl}$*Rragb*$^{fl/fl}$ mice

https://doi.org/10.1038/s41467-024-54344-5

Fig. 1 | Amino acids modulate mTORC1 independent of Rag-GTPases. A, **B** B cells were stimulated with LPS/IL-4/BAFF and cultured with no amino acids (No AA), essential amino acids (EAA), or full amino acids (Full AA) (**A**), or indicated concentrations of amino acids (**B**) overnight. CD98, CD86, p-4EBP1, p-S6, and FSC-A levels were measured by flow cytometry. For CD98, CD86, p-S6, and FSC-A levels, $n = 5$ for each group. $n = 3$ for each group in p-4EBP1 expression. **C**–**F** Tamoxifen was administered to animals intraperitoneally daily for 4 consecutive days. Splenic B cells were purified 7 days after the last tamoxifen injection and stimulated with LPS/IL-4/BAFF. **C** Expression of p-4EBP1, p-S6, CD98, and FSC-A was measured by flow cytometry after overnight activation. Cre^{ER} control (WT) ($n = 4$), Cre^{ER}*Rraga*$^{fl/fl}$*Rragb*$^{fl/fl}$ ($n = 4$), Cre^{ER}*Rptor*$^{fl/fl}$ ($n = 4$). **D** Expression of p-4EBP1, p-S6, p-S6K, AID, and LAMP1 was measured by immunoblot. β-actin was used as the loading control. Arrow indicates non-specific bands. Data represents 3 independent experiments. **E** B cells were labeled with CellTrace violet (CTV) and stimulated with indicated stimuli for 72 h. CTV dilution was measured by flow cytometry. **F** Expression of IgG1 and CTV dilution were examined by flow cytometry. Right, summary of the percentages of divided cells and IgG1$^+$ B cells. WT ($n = 8$), *Cre*^{ER}*Rraga*$^{fl/fl}$*Rragb*$^{fl/fl}$ ($n = 8$), *Cre*^{ER}*Rptor*$^{fl/fl}$ ($n = 4$). **G** Rapamycin was added at 24 h after B cell activation with LPS/IL-4/BAFF. IgG1 expression was examined by flow cytometry at 72 h after activation. Right, summary of the percentages of IgG1$^+$ B cells. The numbers indicate the fold differences of average IgG1$^+$ percentages between WT and RagA/RagB deficient B cells. WT ($n = 5$), *Cre*^{ER}*Rraga*$^{fl/fl}$*Rragb*$^{fl/fl}$ ($n = 4$). Error bars represent mean ± SEM. ns, not significant. $^*p < 0.05$, $^{**}p < 0.01$, $^{***}p < 0.001$, and $^{****}p < 0.0001$, one-way ANOVA (**A**, **B**, and **F**), two-tailed/unpaired Student's *t*-test (**G**), or two-way ANOVA (**C**). Source data are provided as a Source Data file.

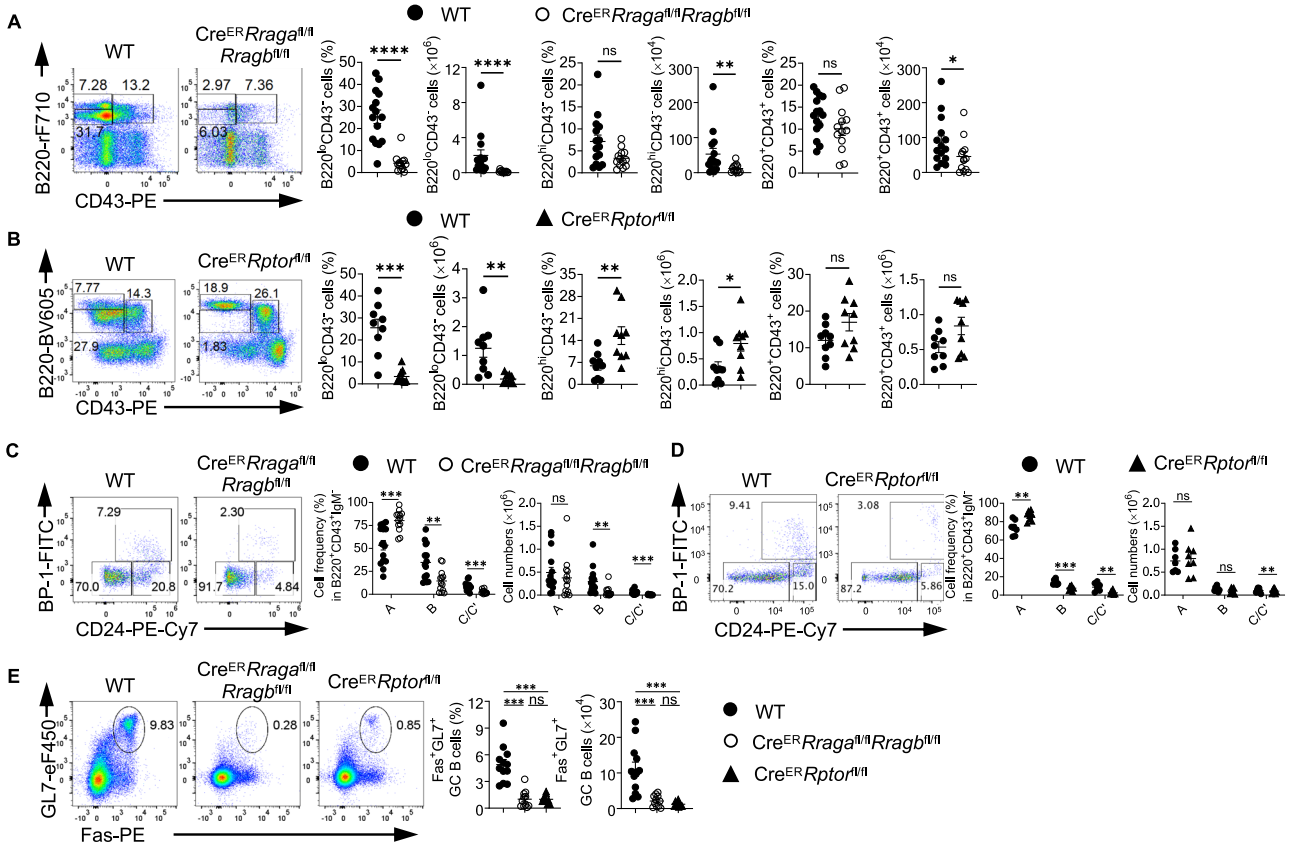

Fig. 2 | Acute deletion of RagA/RagB blocks early B cell development and abolishes germinal center B cells in Peyer's patches. A–**E** Tamoxifen was administered to animals intraperitoneally daily for 4 consecutive days. Mice were analyzed 7 days after the last injection. **A** Expression of B220 and CD43 in bone marrow (BM) lymphocytes from WT ($n = 15$) and *Cre*^{ER}*Rraga*$^{fl/fl}$*Rragb*$^{fl/fl}$ ($n = 13$) mice. Right, summaries of the percentages and numbers of B220^{lo}CD43$^-$, B220^{hi}CD43$^-$ and B220$^+$CD43$^+$ cells. **B** Expression of B220 and CD43 in BM lymphocytes from WT ($n = 9$) and *Cre*^{ER}*Rptor*$^{fl/fl}$ ($n = 9$) mice. Right, summaries of the percentages and numbers of B220^{lo}CD43$^-$, B220^{hi}CD43$^-$ and B220$^+$CD43$^+$ cells. **C** Expression of BP-1 and CD24 in BM B220$^+$CD43$^+$IgM$^-$ B cell precursors from WT ($n = 15$) and *Cre*^{ER}*Rraga*$^{fl/fl}$*Rragb*$^{fl/fl}$ ($n = 13$) mice. Right, summary of the percentages and numbers of fraction A (CD24$^-$BP-1$^-$), fraction B (CD24$^+$BP-1$^-$), and fraction C/C′ (CD24$^+$BP-1$^+$) cells. **D** Expression of BP-1 and CD24 in BM B220$^+$CD43$^+$IgM$^-$ B cell precursors from WT ($n = 7$) and *Cre*^{ER}*Rptor*$^{fl/fl}$ ($n = 8$) mice. Right, summary of the percentages and numbers of fraction A (CD24$^-$BP-1$^-$), fraction B (CD24$^+$BP-1$^-$), and fraction C/C′ (CD24$^+$BP-1$^+$) cells. **E** Expression of GL-7 and Fas in lymphocytes from the Peyer's patches of WT ($n = 12$), *Cre*^{ER}*Rraga*$^{fl/fl}$*Rragb*$^{fl/fl}$ ($n = 11$), and *Cre*^{ER}*Rptor*$^{fl/fl}$ ($n = 9$) mice. Right, summary of the percentages and numbers of GC (GL-7$^+$Fas$^+$) B cells. Data in graphs represent mean ± SEM. ns, not significant. $^*p < 0.05$, $^{**}p < 0.01$, $^{***}p < 0.001$, and $^{****}p < 0.0001$, two-tailed/unpaired Student's *t*-test (**A** and **B**), one-way ANOVA (**E**), two-way ANOVA (**C** and **D**). Source data are provided as a Source Data file.

and Cre^{ER}*Rptor*$^{fl/fl}$ mice following tamoxifen injection (Fig. 2E), indicating that Rag-GTPases and mTORC1 are vital to the formation of GC in PPs. In all cases, RagB deficiency did not affect mature B cell numbers (Supplementary Fig. 1K) or GC formation in PPs (Supplementary Fig. 1L), again demonstrating a redundancy between RagA and RagB.

To study whether the above defects are B cell-intrinsic, we reconstituted lethally irradiated CD45.1$^+$ congenic mice with a 4:1 mixture of bone marrow (BM) recovered from B cell-deficient (μMT) mice and either WT (Cre^{ER}) or Cre^{ER}*Rraga*$^{fl/fl}$*Rragb*$^{fl/fl}$ mice[51,52]. Thus, tamoxifen administration achieved acute B cell-specific deletion of RagA/RagB. Tamoxifen injected μMT:Cre^{ER}*Rraga*$^{fl/fl}$*Rragb*$^{fl/fl}$ mice exhibited reduced B220^{lo}CD43$^-$ pre-B/immature B cells (Supplementary Fig. 2A), modestly reduced frequencies of fraction B and C/C′ B cells (Supplementary Fig. 2B), intact follicular and MZ B cells (Supplementary Fig. 2C), and greatly reduced GC B cells in PPs (Supplementary Fig. 2D). Taken together, B cell-intrinsic Rag-GTPases are critically required for early B cell development and GC formation in PPs.

https://doi.org/10.1038/s41467-024-54344-5

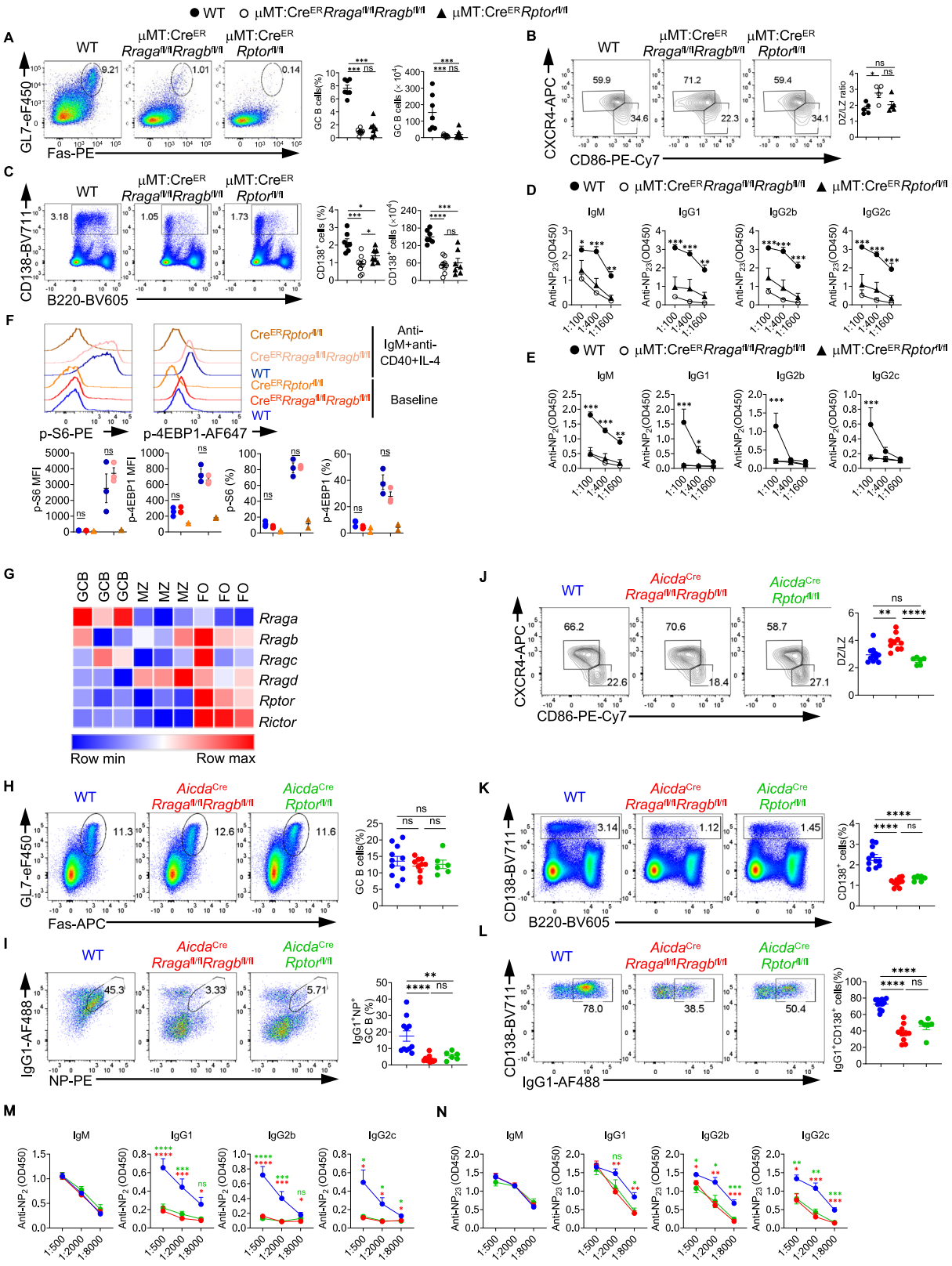

Rag-GTPases are critically required for GC formation and antibody production likely independent of mTORC1

To explore the function of B cell-specific Rag-GTPases following T-dependent immune challenge, we immunized tamoxifen injected μMT:Cre^{ER} (WT), μMT:Cre^{ER}*Rraga*$^{fl/fl}$*Rragb*$^{fl/fl}$ or μMT:Cre^{ER}*Rptor*$^{fl/fl}$ chimera mice with NP-OVA precipitated in alum. Loss of either Rag-GTPases or mTORC1 led to profound loss of GC formation in both spleen and mesenteric lymph node (mLN) (Fig. 3A, Supplementary Fig. 3A) and reduced generation of antigen-specific B cells in both spleen and mLN (Supplementary Fig. 3B, C). Such phenotypes were confirmed with immunofluorescence (Supplementary Fig. 3D). Consistent with the reduction of GC B cells, expression of Bcl6, a transcriptional factor critical for GC reaction[53], was reduced in both mouse strains (Supplementary Fig. 3E). GC is compartmented into LZ

Fig. 3 | Rag-GTPases are critically required for GC formation and antibody production independent of mTORC1. A–**E** Tamoxifen was administered daily for 4 consecutive days followed by NP-OVA/alum immunization on day 11. **A** Expression of GL-7 and Fas in splenic B cells from μMT:Cre^{ER} (WT), μMT:Cre^{ER}*Rraga*$^{fl/fl}$*Rragb*$^{fl/fl}$, and μMT:Cre^{ER}*Rptor*$^{fl/fl}$ mice. Right, summary of the percentages and numbers of GC B cells. **B** Expression of CXCR4 and CD86 in GC B cells. Right, summary of the ratio between dark zone (DZ) (CXCR4^{+}CD86^{-}) and light zone (LZ) (CXCR4^{-}CD86^{+}) cells. **C** Expression of CD138 and B220 in spleens. Right, summary of the percentages and numbers of CD138^{+} cells. **D** ELISA measurement of serum NP_{23}-specific antibodies. WT ($n = 7$), μMT:Cre^{ER}*Rraga*$^{fl/fl}$*Rragb*$^{fl/fl}$ ($n = 8$), and μMT:Cre^{ER}*Rptor*$^{fl/fl}$ ($n = 7$). **E** ELISA measurement of serum NP_{2}-specific antibodies. WT ($n = 5$), μMT:Cre^{ER}*Rraga*$^{fl/fl}$*Rragb*$^{fl/fl}$ ($n = 5$), and μMT:Cre^{ER}*Rptor*$^{fl/fl}$ ($n = 7$). **F** Expression of p-S6 and p-4EBP1 in fresh or overnight activated splenic B cells. **G** Heatmap of the mRNA expression of indicated genes in mouse follicular (FO), marginal zone (MZ), and GC B cells. **H**–**L** NP-OVA was administered to WT ($n = 11$), *Aicda*^{Cre}*Rraga*$^{fl/fl}$*Rragb*$^{fl/fl}$ ($n = 10$), and *Aicda*^{Cre}*Rptor*$^{fl/fl}$ ($n = 6$) mice. **H** Expression of GL-7 and Fas in splenic B cells. Right, summary of the GC B cell percentages. **I** Expression of NP and IgG1 in splenic B cells. Right, summary of the percentages of NP^{+}IgG1^{+} GC B cells. **J** Expression of CXCR4 and CD86 on GC B cells. Right, summary of the DZ/LZ ratios. **K** Expression of CD138 and B220 on splenic lymphocytes. Right, summary of the percentages of CD138^{+} cells. **L** Expression of CD138 and IgG1 in plasmablasts. Right, summary of the percentages of IgG1^{+} plasmablasts. ELISA measurement of serum anti-NP_{2} (**M**) and anti-NP_{23} (**N**) antibodies, WT ($n = 13$), *Aicda*^{Cre}*Rraga*$^{fl/fl}$*Rragb*$^{fl/fl}$ ($n = 8$), and *Aicda*^{Cre}*Rptor*$^{fl/fl}$ ($n = 8$). Data in graphs represent mean ± SEM. ns, not significant. $^{*}p < 0.05$, $^{**}p < 0.01$, $^{***}p < 0.001$, and $^{****}p < 0.0001$, one-way ANOVA (**A**–**C**, **F**, **H**, **I**–**L**), two-way ANOVA (**D**, **E**, **M** and **N**). Source data are provided as a Source Data file.

and DZ. DZ B cells are highly proliferative and undergo somatic hypermutation, while LZ B cells undergo selection and affinity maturation[54]. The ratio of DZ/LZ increased in the remaining GC B cells from μMT:Cre^{ER}*Rraga*$^{fl/fl}$*Rragb*$^{fl/fl}$ mice compared to that in control mice, however, the ratio stayed unchanged in the absence of Raptor (Fig. 3B). Furthermore, plasmablast response in spleen was significantly compromised in both knockout strains, with RagA/RagB deficiency affecting a stronger reduction than mTORC1 deficiency (Fig. 3C). Interestingly, reduced plasmablast frequency was found in the mLNs of immunized μMT:Cre^{ER}*Rraga*$^{fl/fl}$*Rragb*$^{fl/fl}$ mice, but not in those of μMT:Cre^{ER}*Rptor*$^{fl/fl}$ mice (Supplementary Fig. 3F), suggesting a potential tissue specific plasmablast defect in the absence of Raptor. Active-caspase-3 staining showed that RagA/RagB deletion did not affect apoptosis in splenic CD19^{+}, GC and CD138^{+} B cell subsets, and even reduced apoptosis in B cell subsets in the mLN (Supplementary Fig. 3G). Hence, Rag-GTPase deficiency-induced GC and plasmablast differentiation defects are not caused by increased apoptosis. Consistent with the significant reduction of GC and plasmablast generation, total and high-affinity NP-specific antibodies of all classes were highly reduced in both knockout strains. Intriguingly, antibody titers from μMT:Cre^{ER}*Rraga*$^{fl/fl}$*Rragb*$^{fl/fl}$ mice were consistently, although not significantly, lower than those from μMT:Cre^{ER}*Rptor*$^{fl/fl}$ mice (Fig. 3D, E), which could be a reflection of the milder plasmablast defect induced by Raptor deletion relative to that induced by RagA/RagB deletion. Finally, we accessed p-S6 and p-4EBP1 in splenic B cells, either at steady state or after overnight stimulation with anti-IgM/anti-CD40/IL-4, from immunized μMT:Cre^{ER}*Rraga*$^{fl/fl}$*Rragb*$^{fl/fl}$ mice and μMT:Cre^{ER}*Rptor*$^{fl/fl}$ mice. We did not observe significant reduction of mTORC1 activity in RagA/RagB deficient B cells in either condition (Fig. 3F). Taken together, these data indicate an mTORC1 independent function of Rag-GTPases following immunization and illustrate a stronger dependence on Rag-GTPases than on mTORC1 for plasmablast generation.

The above defective GC formation in the absence of RagA/RagB or Raptor could be due to impaired B cell activation. Moreover, we found that *Rraga*, among all Rag family members and mTOR scaffolding molecules, preferentially expressed in GC B cells (Fig. 3G), suggesting a prominent role of RagA in the GC response. To investigate the role of Rag-GTPases post B cell activation, we generated *Aicda*^{Cre}*Rraga*$^{fl/fl}$*Rragb*$^{fl/fl}$ mice and *Aicda*^{Cre}*Rptor*$^{fl/fl}$ mice to ablate RagA/RagB and Raptor after B cell activation, especially in GC B cells[55]. After immunization with NP-OVA/alum, we did not find any apparent alteration of the GC B cell frequencies in the spleens of either *Aicda*^{Cre}*Rraga*$^{fl/fl}$*Rragb*$^{fl/fl}$ mice or *Aicda*^{Cre}*Rptor*$^{fl/fl}$ mice compared with WT mice (Fig. 3H). However, NP^{+}IgG1^{+} GC B cells highly reduced in the spleens of both mouse strains (Fig. 3I), indicating that Rag-GTPases and mTORC1 are both critical for antigen selection in GC B cells. Furthermore, immunized *Aicda*^{Cre}*Rraga*$^{fl/fl}$*Rragb*$^{fl/fl}$ mice harbored higher DZ/LZ ratio, while a slightly reduced DZ/LZ ratio was observed in immunized *Aicda*^{Cre}*Rptor*$^{fl/fl}$ mice (Fig. 3J). We also observed substantially reduced CD138^{+} plasmablast frequency and IgG1 expression on plasmablasts in both *Aicda*^{Cre}*Rraga*$^{fl/fl}$*Rragb*$^{fl/fl}$ and *Aicda*^{Cre}*Rptor*$^{fl/fl}$ mice (Fig. 3K, L). Measurement of NP-specific antibodies showed decreased titers of high-affinity and total IgG isotypes, but not IgM, from the sera of either mouse strain (Fig. 3M, N). Altogether, these data demonstrate that both Rag-GTPases and mTORC1 are required for TD antigen-induced GC formation. But Rag-GTPases and mTORC1 likely employ distinct mechanisms to promote plasmablast formation and maintain GC dynamics.

Rag-GTPases support mitochondrial fitness during B cell activation, likely independent of mTORC1

B cell activation is accompanied by extensive metabolic reprogramming including glycolytic switches and activation of mitochondrial oxidative phosphorylation[56]. We examined mitochondrial respiration and glycolysis in activated B cells by measuring oxygen consumption rate (OCR) and extracellular acidification rate (ECAR), respectively. Deficiency of either RagA/RagB or Raptor led to significantly decreased OCR (Fig. 4A). Raptor deficiency strongly suppressed glycolysis, while RagA/RagB deficient B cells had a slight reduction of ECAR (Fig. 4B). [3-^{3}H]-glucose labeling assay confirmed the profound glycolytic defect in Raptor deficient B cells. It showed a modest but significant reduction of glucose metabolism in RagA/RagB deficient B cells (Fig. 4C). Thus, Rag-GTPases are critical for B cell metabolism, especially oxidative phosphorylation. Interestingly, despite a relatively stronger reduction of OCR in Raptor deficient B cells, RagA/RagB deficiency, but not Raptor deficiency, resulted in significant reduction of mitochondrial membrane potential, measured by tetramethylrhodamine methyl ester (TMRM) (Fig. 4D) and MitoTracker Deep Red (MTDR) (Fig. 4E)[57,58], as well as mitochondrial reactive oxygen species (ROS) measured by MitoSox (Fig. 4F), suggesting that loss of Rag-GTPases might lead to defective mitochondria and subsequent reduced mitochondrial activity, while mTORC1 deficiency compromises OCR through distinct mechanisms. Consistent with this hypothesis, rapamycin treatment did not affect TMRM and MTDR staining in WT B cells, nor did it further decrease mitochondrial membrane potential in RagA/RagB deficient B cells (Supplementary Fig. 4A, B). Moreover, examination of mitochondrial phenotypes in vivo revealed that GC B cells from the immunized *Aicda*^{Cre}*Rraga*$^{fl/fl}$*Rragb*$^{fl/fl}$ mice, but not *Aicda*^{Cre}*Rptor*$^{fl/fl}$ mice, showed significantly reduced mitochondrial membrane potential and ROS level (Fig. 4G-H). Previous studies indicated that mTORC1 controlled the expression of key transcription factors for mitochondrial biogenesis programs, including PGC-1α and TFAM[59,60]. Indeed, expression of PGC-1α (Fig. 4I), TFAM (Fig. 4J)[61], and COXI (Fig. 4K), a member of the mitochondrial respiratory chain were all significantly decreased in Raptor deficient B cells, but not in RagA/RagB deficient B cells. Collectively, Rag-GTPase deficiency in B cells impairs mitochondrial metabolism associated with reduced mitochondrial membrane potential and mitochondrial ROS, which are distinctive from Raptor deficient B cells.

https://doi.org/10.1038/s41467-024-54344-5

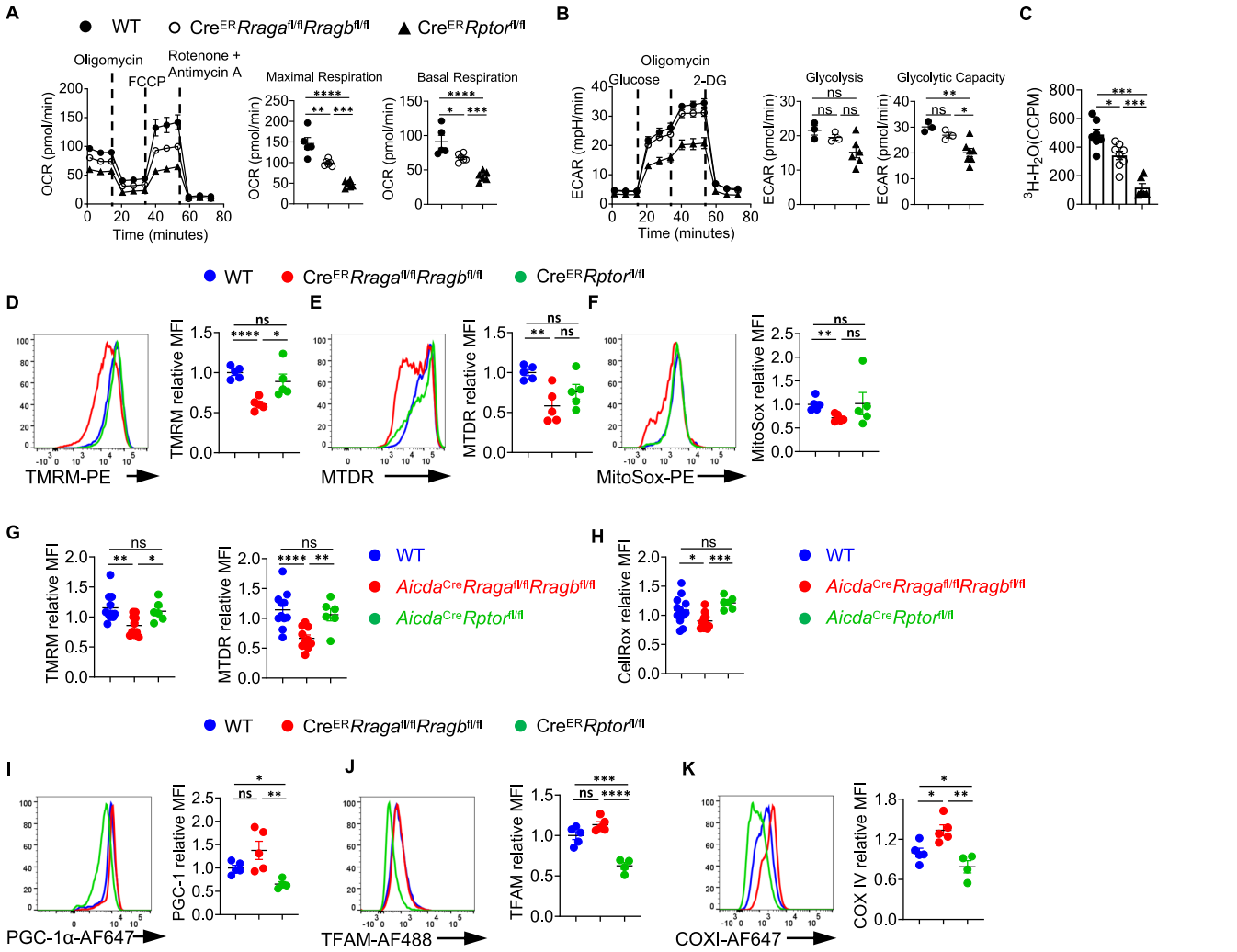

Fig. 4 | Rag-GTPases regulate B cell activation and mitochondrial metabolism differently from canonical mTORC1. A–**F**, **I**–**K** Splenic B cells were purified from tamoxifen-treated WT, *Cre^{ER}Rraga$^{fl/fl}$Rragb$^{fl/fl}$*, and *Cre^{ER}Rptor$^{fl/fl}$* mice, and cultured with LPS/IL-4/BAFF for 72 h. Mitostress assay (**A**), and glycolytic stress assay (**B**) were performed on a Seahorse XFe96 bioanalyzer. **C** Glycolytic flux was examined using LPS/IL-4/BAFF activated B cells by measuring the detritiation of [3-^{3}H] glucose. Representative flow plots of tetramethylrhodamine methyl ester (TMRM) (**D**, 5 mice per group), MitoTracker Deep Red (MTDR) (**E**, 5 mice per group), and MitoSox (**F**, 5 mice per group) stainings were shown. Summaries of the mean fluorescence intensity (MFI) of each staining (relative to WT) were on the right. **G** Summaries of the MFIs of TMRM and MTDR staining (relative to WT) on GC B cells from the spleens of immunized mice. **H** Summary of the MFIs of CellRox staining (relative to WT) on GC B cells from the spleens of immunized. Representative flow plots of PGC-1α (**I**), TFAM (**J**), and COXI (**K**) stainings were shown. Summaries of the MFI of each staining (relative to WT) were on the right. Data in graphs represent mean ± SEM. ns, not significant. *$p < 0.05$, **$p < 0.01$, ***$p < 0.001$, and ****$p < 0.0001$, one-way ANOVA (**A**–**K**). Source data are provided as a Source Data file.

Rag-GTPase deficiency leads to TFEB/TFE3 overactivation and abnormal mitophagy

To probe the molecular mechanisms underlying the above metabolic defects, we conducted RNA sequencing using activated B cells and GC B cells. Gene set enrichment analysis (GSEA) identified the KEGG lysosome pathway and putative TFEB target genes as two of the top enriched pathways in RagA/RagB deficient B cells (Fig. 5A-B, Supplementary Fig. 4C). Many lysosomal genes were upregulated in the RagA/RagB deficient B cells (Supplementary Fig. 4D), such as *Lamp1*, *Atp6ap1*, *Atp6v1h* and *Ctsa*. RNA sequencing using GC B cells from the immunized *Aicda^{Cre}Rraga$^{fl/fl}$Rragb$^{fl/fl}$* mice and *Aicda^{Cre}Rptor$^{fl/fl}$* mice demonstrated a relatively effective deletion of *Rraga* and *Rptor* (Supplementary Fig. 4E). The principal component analysis (PCA) plot showed that WT and Raptor deficient cells were closer to each other, while both were distant from Rag-GTPases deficient cells (Supplementary Fig. 4F). Consistent with this observation, Venn diagram of differentially expressed genes (DEG) illustrated that majority of DEGs were from the RagA/RagB KO vs WT comparison (85.7%, 1812/2114), and less than 10% of DEGs (175/2114) were identified comparing Raptor KO with WT (Fig. 5C, Supplementary Fig. 4G). There were more DEGs shared between RagA/RagB KO vs WT and RagA/RagB KO vs Raptor KO than between Raptor KO vs WT, indicating a stronger impact of Rag-GTPase deficiency on GC B cell transcriptome than Raptor deficiency. GSEA identified KEGG lysosome pathway as the top enriched pathway comparing RagA/RagB KO to WT GC B cells (Fig. 5D), or comparing RagA/RagB KO to Raptor KO GC B cells (Fig. 5E), while no significant enrichment of KEGG lysosome was observed when comparing GC B cells from *Aicda^{Cre}Rptor$^{fl/fl}$* and WT mice (Fig. 5F), suggesting lysosomal activation in RagA/RagB deficient, but not in Raptor deficient, GC B cells. Therefore, Rag-GTPases and mTORC1 utilize distinct mechanisms to maintain GC reaction post B cell activation, one of which was likely TFEB regulation.

To directly examine TFEB function activity, we measured the mRNA levels of TFEB target genes, including *Lamp1*, *Rragd*, and *Flcn*. Consistent with the RNA sequencing data, TFEB target gene expression was significantly increased in RagA/RagB deficient B cells, but not in

https://doi.org/10.1038/s41467-024-54344-5

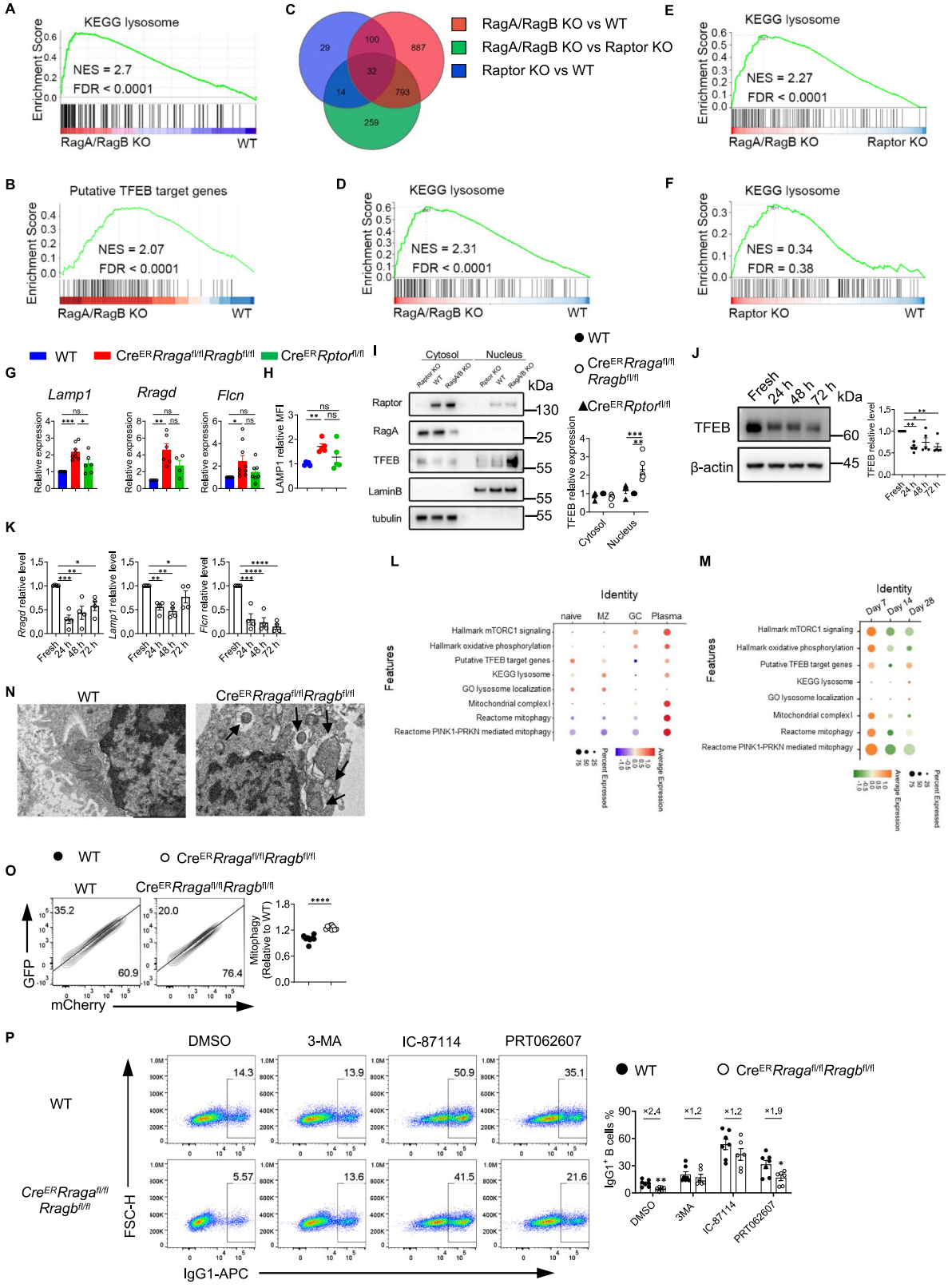

Raptor deficient B cells (Fig. 5G). We also confirmed that LAMP1 protein expression was increased in the absence of Rag-GTPases, but not Raptor (Figs. 5H, 1D). Importantly, we observed increased TFEB and TFE3 nuclear localization in RagA/RagB deficient B cells, but not in Raptor deficient B cells (Fig. 5I, Supplementary Fig. 4H). Therefore, Rag-GTPases, but not mTORC1, constrain TFEB/TFE3 activity during B cell activation.

To further gain insight into the possible functions of TFEB during B cell activation, we first examined TFEB protein expression kinetics in in vitro activated B cells. TFEB protein had the highest expression in naïve B cells and its expression declined over time (Fig. 5J). Meanwhile, we observed reduced expression of *Lamp1, Rragd*, and *Flcn* (Fig. 5K), indicating an association between B cell activation and reduced TFEB activity. To further investigate the TFEB activity in vivo, we re-analyzed

Fig. 5 | RagA/RagB deficiency leads to TFEB/TFE3 overactivation and abnormal mitophagy. A RNA sequencing was performed on 72-h activated B cells. Gene set enrichment analysis (GSEA) was conducted using differentially expressed genes (DEGs) with KEGG lysosome pathway plotted. **B** The enrichment of putative TFEB target genes. **C** RNA sequencing was performed on sorted germinal center (GC) B cells. Venn diagram of three DEG comparisons was presented. **D**–**F** GSEA was performed using the DEGs between indicated genotypes with KEGG lysosome pathway enrichment between indicated genotypes presented. **G** qRT-PCR of *Lamp1*, *Rragd*, and *Flcn* expression. **H** Flow cytometry of LAMP1 expression, $n = 5$ mice per group. **I** Immunoblot of Raptor, RagA, and TFEB expression. Cytosolic and nuclear proteins were isolated from activated B cells. Lamin-B, nuclear control, tubulin, cytosol control. WT ($n = 5$), $Cre^{ER}Rraga^{fl/fl}Rragb^{fl/fl}$ ($n = 7$), and $Cre^{ER}Rptor^{fl/fl}$ ($n = 4$). **J** Expression of TFEB at indicated time-points ($n = 5$ for each condition). Right, summary of relative TFEB expression (normalized to fresh). **K** qRT-PCR of *Lamp1*, *Rragd*, and *Flcn* expression at indicated time-points. $n = 4$ for each condition. **L**, **M** Published scRNAseq dataset (E-MTAB-9478) was reanalyzed with gene signatures in naïve, marginal zone (MZ), GC B cells, and plasma cells presented (**L**). Gene signatures in GC B cells at different time points (**M**). **N** Transmission electron microscopy (TEM) of activated B cells. Arrows indicate mitochondria surrounded by double-layer structures. Scale bar, 2 μm. **O** GFP and mCherry expression with Mito-QC transduction. Right, summary of the normalized mCherry percentages (Relative to mCherry percentage in WT). WT ($n = 8$), and $Cre^{ER}Rraga^{fl/fl}Rragb^{fl/fl}$ ($n = 10$). **P** IgG1 expression on B cells stimulated in the presence of indicated inhibitors. Right, summary of $IgG1^+$ B cell percentages. WT ($n = 7$), $Cre^{ER}Rraga^{fl/fl}Rragb^{fl/fl}$ ($n = 6$). Data represents at least 3 (**G**–**K**, **O**, **P**) and 2 (**N**) independent experiments. Data in graphs represent mean ± SEM. ns, not significant. $^*p < 0.05$, $^{**}p < 0.01$, $^{***}p < 0.001$, and $^{****}p < 0.0001$, one-way ANOVA (**G**–**K**), two-tailed/unpaired Student's *t*-test (**O** and **P**). Source data are provided as a Source Data file.

the public database and evaluated the expression of mTORC1 signaling signatures, putative TFEB target genes[62], oxidative phosphorylation, and lysosome-related genes in naïve B cells, MZ B cells, GC B cells and plasma cells (Fig. 5L) and GC B cells at different time points (Fig. 5M) from influenza-infected mice. While mTORC1 signatures, oxidative phosphorylation, and mitochondrial complex I were highly enriched in plasma cells, TFEB targets and lysosome-related genes were enriched in naïve and MZ B cells, and they had the lowest expression in GC B cells (Fig. 5L). In the time-course analysis, TFEB target gene expression declined at day 14 compared to day 7 before recovering at day 28 (Fig. 5M). The expression pattern and kinetics of TFEB activity were not reciprocal to mTORC1 activation, suggesting that they could be independent to each other in B cells. Taken together, our results suggest that B cell activation and differentiation are associated with the decline of TFEB activity, which might be enforced by Rag-GTPases.

TFEB has been implicated in the regulation of mitophagy[63,64]. Yet, the function of TFEB and mitophagy during B cell activation remains unknown. Transmission electron microscopy (TEM) analysis revealed mitochondria encircled with double membrane structures, morphology consistent with mitophagy, in RagA/RagB deficient B cells (Fig. 5N). To confirm the mitophagy phenotype, we introduced Mito-QC, a mitophagy reporter, which is a construct expressing an mCherry-GFP tag attached to mitochondrial fission protein 1 (FIS1, residues 101–152) on the outer mitochondrial membrane[65]. Upon mitophagy, mitochondria are delivered to lysosomes from autophagosomes, where the GFP signal is quenched by the low lysosomal pH, resulting in only red fluorescence (mCherry signals). In accordance with the TEM data, we observed increased mCherry signals in RagA/RagB deficient B cells (Fig. 5O). Thus, Rag-GTPase deficiency is associated with increased TFEB activity and mitophagy in B cells. To further gain insight into the role of mitophagy in B cell activation, we treated B cells with several putative mitophagy activators including CMPD-39, MF095, and Urolitin A, all of which significantly reduced IgG1 expression on B cells without apparently affecting B cell proliferation (Supplementary Fig. 5A, B). Conversely, putative mitophagy inhibitors including 3-MA, IC-87114, and PRT062607 not only increased the IgG1 expression on WT B cells but also partially restored IgG1 expression on RagA/RagB deficient B cells without affecting cell proliferation (Fig. 5P and Supplementary Fig. 5C–F). Therefore, excessive mitophagy could be detrimental to B cell activation. Abnormally increased mitophagy activity could underly some of the B cell activation defects in the absence of Rag-GTPase.

TFEB/TFE3 overactivation is responsible for the abnormal mitophagy and impaired mitochondrial fitness in RagA/RagB deficient B cells

To test whether TFEB overactivation can directly control mitochondrial phenotypes and B cell activation, we retrovirally overexpressed WT TFEB or constitutive active TFEB (Ca TFEB) carrying S142/211A mutation (Supplementary Fig. 6A)[66], with comparable transduction efficiency (Supplementary Fig. 6B). WT TFEB and Ca TFEB overexpression promoted TFEB activation in a graded manner, as measured by the expression of TFEB target genes (Fig. 6A). They also reduced $IgG1^+$ class switching (Fig. 6B) and $CD138^+$ expression (Supplementary Fig. 6C) in a graded manner, without overtly affecting B cell proliferation and mTORC1 activity (Supplementary Fig. 6D, E). We observed similar phenotypes when we pharmacologically stimulated TFEB using curcumin analog C1, a novel mTOR-independent activator of TFEB[67] (Supplementary Fig. 6F, G). Hence, TFEB overactivation suppresses class switch and CD138 expression in vitro.

RNA sequencing revealed the enrichment of lysosome pathway in Ca TFEB transduced B cells (Supplementary Fig. 6H). There was a substantial overlap between the DEGs from the RagA/RagB deficient B cells and those from Ca TFEB expressing B cells: 70% downregulated genes (882 genes) and 75% upregulated genes (899 genes) were shared (Fig. 6C), suggesting that TFEB overactivation might account for a significant portion of the DEGs in RagA/RagB deficient B cells. Like RagA/RagB deficient B cells, TFEB overactivation led to striking reductions of mitochondrial membrane potential (TMRM and MTDR, Fig. 6D) and mitochondrial ROS (MitoSox, Fig. 6E), and increased LAMP1 expression (Fig. 6F). Importantly, TEM analysis revealed the increased mitochondrial morphology consistent with mitophagy in Ca TFEB transduced B cells (Fig. 6G). Of note, TFEB overactivation promoted mitophagy likely through PINK1-PRKN/Parkin mediated pathway because we detected a significant increase of ubiquitin (Ub) phosphorylation at Ser65 (p-S65-Ub)[68] (Fig. 6H). Thus, TFEB activation is sufficient to suppress mitochondrial activity associated with abnormal mitophagy in B cells.

To establish whether TFEB overactivation was responsible for B cell activation and mitochondrial defects observed in RagA/RagB deficient B cells, we generated dominant negative TFEB (TFEB TDN), which contained the helix-loop-helix–leucine zipper dimerization domains but lacked the DNA-binding basic region and transcription activation domains[45]. TFEB TDN transduction partially suppressed TFEB overactivation and partially rescued the reduced $IgG1^+$ expression in RagA/RagB deficient B cells (Supplementary Fig. 6I, J). Moreover, TFEB TDN partially restored mitochondrial membrane potential (Fig. 6I-J) and MitoSox level in RagA/RagB deficient B cells (Supplementary Fig. 6K). These data indicate that TFEB overactivation could be partly responsible for the mitochondrial defects induced by RagA/RagB deficiency in vitro.

To investigate if genetic inactivation of TFEB can restore B cell mitochondrial fitness in the absence of Rag-GTPases, we crossed $Cre^{ER}Rraga^{fl/fl}Rragb^{fl/fl}$ mice with a $Tfeb^{fl/fl}$ allele to generate $Cre^{ER}Rraga^{fl/fl}Rragb^{fl/fl}Tfeb^{fl/fl}$ mice. As expected, loss of TFEB greatly reduced the expression of *Tfeb* and many TEFB target genes in RagA/RagB deficient B cells (Supplementary Fig. 6L). TFEB deletion restored the reduced IgG1 class switch (Fig. 6K), mitochondrial membrane potential (Fig. 6L), mitochondrial ROS (Fig. 6M), and reversed the increased

https://doi.org/10.1038/s41467-024-54344-5

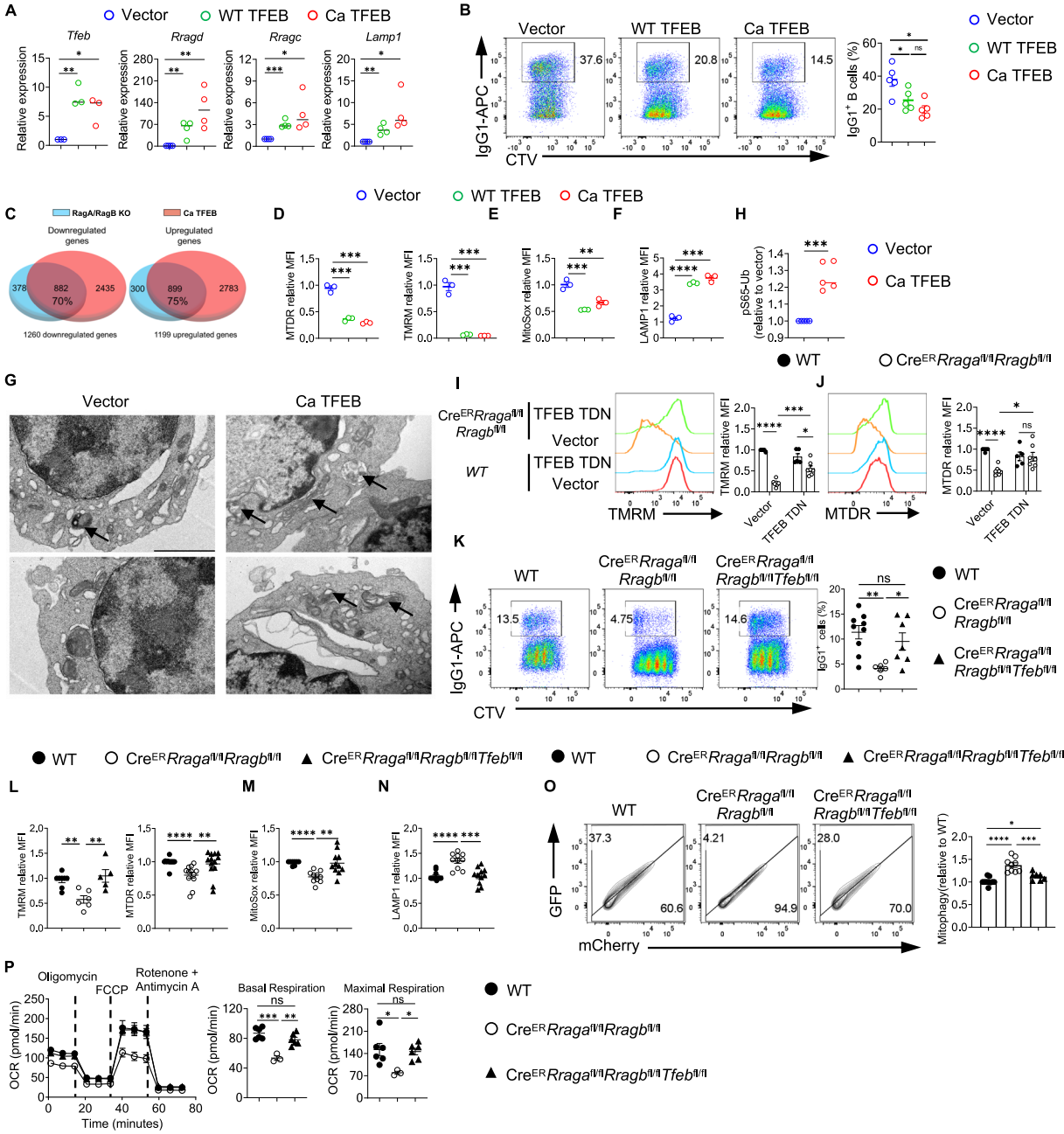

Fig. 6 | TFEB/TFE3 overactivation is responsible for the abnormal mitophagy and impaired mitochondrial fitness in RagA/RagB deficient B cells. A qRT-PCR of *Tfeb*, *Rragd*, *Rragc*, and *Lamp1* expression. GFP$^+$ B cells were sorted from vector, WT TFEB, and Ca TFEB transduced B cells. **B** Expression of IgG1 and Celltrace violet (CTV) in transduced B cells. $n = 4$ for each group. **C** Venn diagrams highlight the overlapping gene numbers in downregulated DEGs (left) and upregulated DEGs (right) between Rag KO vs WT comparison and Ca TFEB vs vector comparison. **D** Summaries of the relative MTDR (left) and TMRM (right) MFIs. $n = 3$ for each group. **E** Summary of the relative MitoSox MFIs. $n = 3$ for each group. **F** Summary of the relative LAMP1 MFIs. $n = 3$ for each group. **G** Transmission electron microscope (TEM) of sorted vector or Ca TFEB transduced B cells. Arrows indicate mitochondria surrounded by double-layer structures. scale bar, 2 µm. (**H**) ELISA of pS65-Ub levels in sorted vector or Ca TFEB transduced B cells. $n = 5$ for each group. Flow cytometry of TMRM (**I**) or MTDR (**J**) staining of vector or TFEB TDN transduced B cells. WT ($n = 5$), *Cre^{ER}Rraga$^{fl/fl}$Ragb$^{fl/fl}$* ($n = 7$). **K** Flow cytometry of IgG1 and CTV. B cells from indicated genotypes were activated with LPS/IL-4/BAFF for 3 days. TMRM or MTDR (**L**), MitoSox (**M**), or LAMP1 (**N**) were measured by flow cytometry. **O** GFP and mCherry expression in B cells with Mito-QC transduction. **P** B cells from the indicated mice were purified and activated with LPS/IL-4/BAFF for 72 h. Mito stress assay was performed on a Seahorse XFe96 analyzer. Right, summaries of the basal respiration and maximal respiration. Data in graphs represent mean ± SEM. ns, not significant. $^*p < 0.05$, $^{**}p < 0.01$, $^{***}p < 0.001$, and $^{****}p < 0.0001$, one-way ANOVA (**A**, **B**, **D**–**F**, **K**–**P**), two-way ANOVA (**I** and **J**), two-tailed/unpaired Student's *t*-test (**H**). Source data are provided as a Source Data file.

expression of LAMP1 (Fig. 6N). Importantly, TFEB deficiency prevented the abnormal mitophagy measured by Mito-QC assay (Fig. 6O). Finally, the reduced mitochondrial metabolism, measured by OCR, induced by RagA/RagB loss was fully restored by TFEB deletion (Fig. 6P) without apparent impact on mTORC1 activity measured by p-S6 and p-4EBP1 (Supplementary Fig. 6M). Altogether, these data demonstrated that Rag-GTPases constrain TFEB/TFE3 activity to prevent abnormal mitophagy and maintain mitochondrial fitness in B cells in vitro.

Rag-GTPase-TFEB/TFE3 axis modulates humoral immunity in a context-dependent manner

We next sought to assess the impact of TFEB deletion on Cre^{ER}*Rraga*$^{fl/fl}$*Rragb*$^{fl/fl}$ mice in vivo. TFEB deletion restored the reduced frequencies of fractions B and fraction C/C′ precursors, but not the blockage of the pro-B to pre-B transition, nor the reduced GC formation in PPs caused by RagA/RagB deficiency (Supplementary Fig. 7A–C). To evaluate the humoral immune responses against TD antigens, we immunized tamoxifen injected μMT:Cre^{ER}*Rraga*$^{fl/fl}$*Rragb*$^{fl/fl}$*Tfeb*$^{fl/fl}$ mice and μMT:Cre^{ER}*Rraga*$^{fl/fl}$*Rragb*$^{fl/fl}$ mice with NP-OVA/alum. TFEB deletion did not restore the reduced GC B cells, plasmablasts, NP^{+}IgG1^{+} GC B cells, IgG1^{+}CD138^{+} cells, and the production of NP-specific antibodies in the absence of RagA/RagB (Supplementary Fig. 7D–I). Thus, TFEB deletion was not sufficient to restore early B cell development, GC formation in PPs, and humoral responses towards TD antigens in the absence of Rag-GTPases.

To investigate immune response to TI-antigen, we immunized tamoxifen injected μMT:Cre^{ER}*Rraga*$^{fl/fl}$*Rragb*$^{fl/fl}$*Tfeb*$^{fl/fl}$ mice and μMT:Cre^{ER}*Rraga*$^{fl/fl}$*Rragb*$^{fl/fl}$ mice with TNP-LPS. RagA/RagB deletion led to significant reduction of plasmablast generation and TNP-specific antibody production, both of which were restored by TFEB deletion (Supplementary Fig. 7J, K). Interestingly, we observed that plasmablasts generated by TNP-LPS immunization exhibited greater mitochondrial membrane potential, measured by TMRM and MTDR, than those generated by NP-OVA immunization (Supplementary Fig. 7L), suggesting a potentially higher mitochondrial metabolism in TNP-LPS induced plasmablasts than NP-OVA induced plasmablasts. Thus, our data indicate that TFEB overactivation is responsible for the impaired TI-antigen responses, but not the reduced TD-antigen responses, pro-B to pre-B transition, or GC formation in PPs in the absence of Rag-GTPases.

RagA/RagB deficiency led to overactivation of both TFEB and TFE3 (Fig. 5I, Supplementary Fig. 4H). To address the potential redundancy between TFEB and TFE3, we generated Cre^{ER}*Rraga*$^{fl/fl}$*Rragb*$^{fl/fl}$*Tfeb*$^{fl/fl}$*Tfe3*$^{-/-}$ mice (Supplementary Fig. 1A). Strikingly, we found that TFEB/TFE3 deletion significantly restored the reduction of B220^{lo}CD43^{-} pre-B/immature B cells and fraction A and fraction C/C′ frequencies in the BM (Fig. 7A, B), and GC formation in PPs (Fig. 7C) in the absence of RagA/RagB, demonstrating a non-redundant role between TFE3 and TFEB during early B cell development and spontaneous GC formation in mucosal site under the control of Rag-GTPases. Like TFEB deletion, TFEB/TFE3 deletion restored most of the in vitro activation and metabolic defects in RagA/RagB deficient B cells, including reduced IgG1 expression (Fig. 7D), mitochondrial membrane potential (Fig. 7E), ROS level (Fig. 7F) and increased LAMP1 expression (Fig. 7G), as well as the reduced OCR (Fig. 7H). Next, we immunized tamoxifen injected μMT:Cre^{ER}*Rraga*$^{fl/fl}$*Rragb*$^{fl/fl}$*Tfeb*$^{fl/fl}$*Tfe3*$^{-/-}$ mice and μMT:Cre^{ER}*Rraga*$^{fl/fl}$*Rragb*$^{fl/fl}$ mice with NP-OVA/alum or TNP-LPS. TFEB/TFE3 deficiency was not able to rescue the reduced GC and plasmablast formation upon NP-OVA immunization in the absence of RagA/RagB (Fig. 7I–J). However, the reduced responses towards TNP-LPS immunization in RagA/RagB deficient B cells were nearly restored by TFEB/TFE3 deletion (Fig. 7K-L). Taken together, these data reveal non-redundant functions for TFEB and TFE3 in B cell development and GC formation in mucosal site. They support the notion that Rag-GTPase-TFEB/TFE3 axis regulates B cell development, activation, and differentiation under different immune contexts.

Discussion

Research in childhood malnutrition has long highlighted the impact of nutrient availability and immunity. Yet, the complex interplay between systemic metabolic dysregulation and immune system hampers the mechanistic understanding of nutrient sensing and immunometabolism in adaptive immune system[69]. Recent studies have established Rag-GTPases as a key sensor for amino acids. Rag-GTPases primarily control mTORC1 and TFEB/TFE3 activity. In the current study, we utilized genetic models to establish the mechanisms through which Rag-GTPases suppress TFEB/TFE3 in B cell development and activation in a likely mTORC1-independent manner.

The relationship between Rag-GTPases and mTORC1 has been contentious. Rag-GTPases were initially found to be necessary and sufficient for mTORC1 activation, including in immune cells[21,23,24,32]. However, amino acids can engage mTORC1 independent of Rag-GTPases[30]. Our study demonstrated that Rag-GTPases are not necessary for mTORC1 activation in B cells. Our observations join several recent studies to illustrate the relationship between Rag-GTPases and mTORC1 is cell-type and context-dependent: Rag-GTPases can be sufficient but not necessary for mTORC1 activation in B cells[24,25]. Furthermore, Rag-GTPases and mTORC1 in GC B cells are critical for antigen selection and antibody affinity maturation. Yet only Rag-GTPases, but not mTORC1, modulate DZ vs LZ distribution and lysosome metabolism in GC B cells. Finally, Rag-GTPases play a more prominent role in supporting plasmablast formation than mTORC1, whose underlying mechanisms remain to be investigated. These results uncover the distinct requirements of Rag-GTPases and mTORC1 in humoral immunity. Both Rag-GTPase and mTORC1 are modulated by amino acids. Specific amino acids have been identified to promote mTORC1 in different mammalian cells[32,70]. Thus, it is plausible that different amino acids may provide different upstream signals and differentially regulate Rag-GTPase and mTORC1. This hypothesis awaits future investigations.

While recent advances in immunometabolism field have identified certain metabolic requirements during mature B cell activation, much less is known about metabolic regulations during B cell development, spontaneous GC reaction in mucosal site, and humoral responses towards TD and TI antigens. Our data establish a Rag-GTPase-TFEB/TFE3-mitophagy pathway that controls mitochondrial fitness in B cells. Instead of promoting mTORC1, Rag-GTPases suppress TFEB/TFE3 activity following B cell activation. Deficiency of Rag-GTPases leads to TFEB/TFE3 nuclear accumulation and overactivation, which induces mitophagy and reduces mitochondrial membrane potential and mitochondrial oxidative phosphorylation. Importantly, our data demonstrate a key differential requirement of TFEB/TFE3 transcription factors between TD and TI responses, i.e., Rag-GTPase mediated TFEB/TFE3 suppression is critical for TI response, but a Rag-GTPase dependent but TFEB/TFE3 independent mechanism is required for TD response. The molecular mechanisms governing TI responses are much less understood compared to those regulating TD responses. A recent study showed that TD, but not TI, responses depend on LDHA-mediated glycolysis[10]. Here, our study demonstrated that mitochondrial integrity mediated by Rag-GTPase-TFEB/TFE3 axis is critical for TI response but may not be sufficient for TD response. The TFEB/TFE3 independent but Rag-GTPase dependent mechanisms for TD response await future study. The higher mitochondrial membrane potential in plasmablasts induced by TI-antigen than TD-antigen suggests a possibility that TI-response might have a greater reliance on mitochondrial metabolism than TD-response, consistent with a recent study[71]. More research is warranted to test this proposition. Thus, our investigation helps fill a critical knowledge gap and further highlight the distinct signaling and metabolic requirements between TD and TI responses.

Finally, our study unveils overlapping and non-redundant functions between TFEB and TFE3 in B cells. While deletion of TFEB alone or both TFEB and TFE3 can restore the impaired antibody response to TI antigens in RagA/RagB deficient B cells, deletion of both TFEB and TFE3 is needed to rectify early B cell development defects and reduced GC formation in PPs in the absence of Rag-GTPases. Altogether, our investigations illustrate specific metabolic and signaling requirements in the lifetime of B cells at different stages and different anatomic locations coordinated by Rag-GTPase-TFEB/TFE3 signaling axis. Another known regulator of TFEB and mTORC1 is folliculin (FLCN),

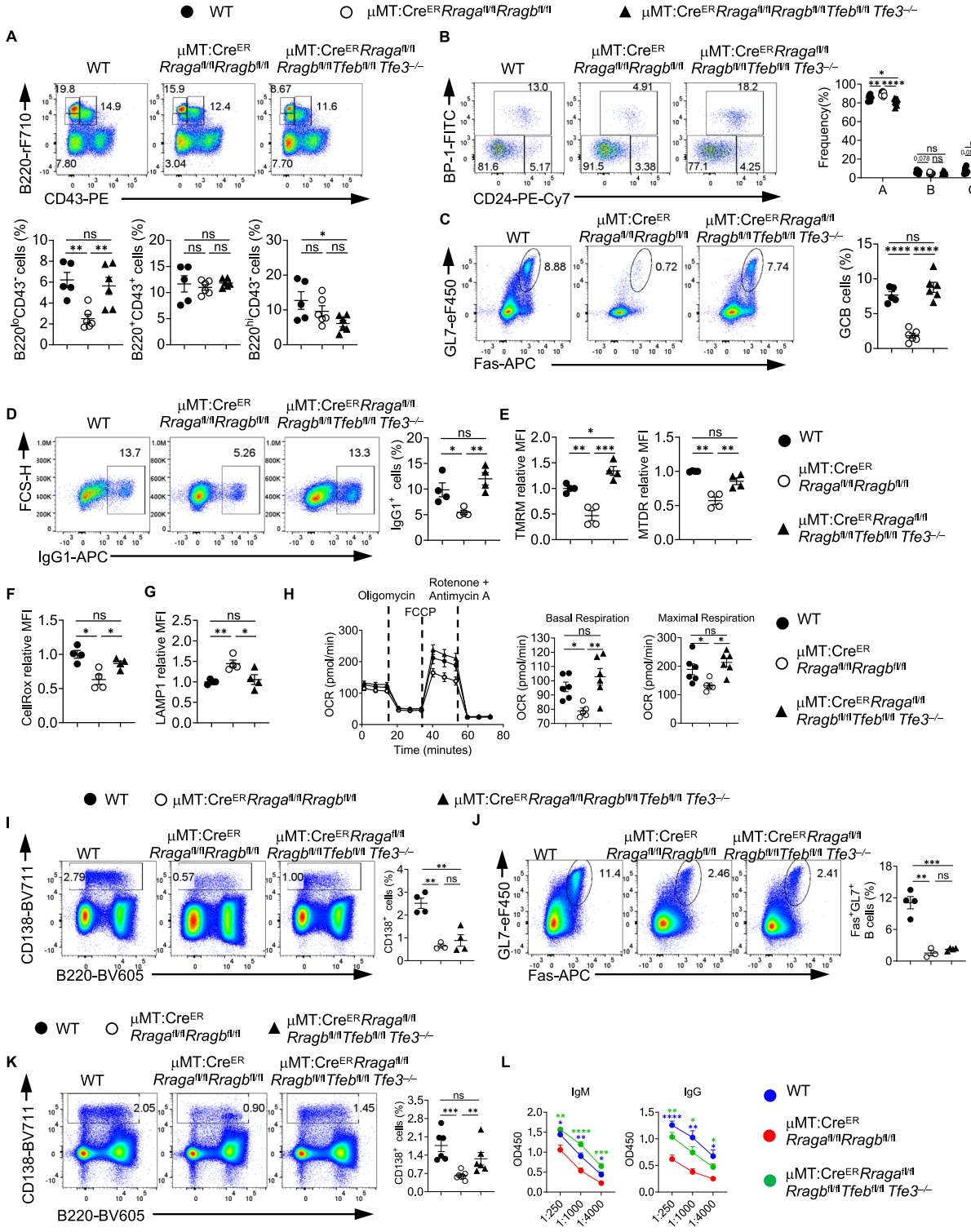

which also directly interacts with Rag-GTPase[22,42]. Its contribution to Rag-GTPase-TFEB/TFE3 mediated mitochondrial metabolism in B cells requires future investigation.

Methods

Mice

ROSA26-Cre-ERT2, *Rraga*$^{fl/fl}$*Rragb*$^{fl/fl}$, *Rptor*$^{fl/fl}$ mice have been previously described[27,34]. CD45.1^{+} (RRID: IMSR_JAX:002014), C57BL/6J (RRID: IMSR_JAX:000664), and *Rag1*$^{-/-}$ (RRID: IMSR_JAX:002216), B6.129S2-*Ighm*^{tm1Cgn}/J (RRID:IMSR_JAX:002288) and B6.129P2-*Aicda*$^{tm1(cre)Mnz}$/J (RRID:IMSR_JAX:007770) mice were purchased from the Jackson Laboratory. *Tfeb*$^{fl/fl}$ mouse was a gift from Dr. Andrea Ballabio (Telethon Institute of Genetics and Medicine)[72]. *Tfe3*$^{-/-}$ mouse was a gift from Dr. Ming O. Li (Memorial Sloan Kettering Cancer Center)[31]. *Cre*^{ER}*Rraga*$^{fl/fl}$*Rragb*$^{fl/fl}$ (*Rragb*$^{fl/fl}$ denotes male hemizygous or female homozygous mice for *Rragb* because *Rragb* is located on the X-chromosome). *Cre*^{ER}*Rragb*$^{fl/fl}$ mice, *Cre*^{ER}*Rptor*$^{fl/fl}$, *Cre*^{ER}*Rraga*$^{fl/fl}$*Rragb*$^{fl/fl}$*Tfeb*$^{fl/fl}$, *Cre*^{ER}*Rraga*$^{fl/fl}$*Rragb*$^{fl/fl}$*Tfeb*$^{fl/fl}$*Tfe3*$^{-/-}$ and age- and gender-matched littermate controls were analyzed at the indicated ages. Bone marrow (BM) chimeras were generated by transferring T cell-depleted bone

Fig. 7 | Rag-GTPases-TFEB/TFE3 axis modulates humoral immunity in a context dependent manner. A Flow cytometry of CD43 and B220 expression on BM cells. Below, summaries of $B220^{lo}CD43^{-}$, $B220^{hi}CD43^{-}$ and $B220^{+}CD43^{+}$ cell frequencies. **B** Flow cytometry of BP-1 and CD24 expression in BM $B220^{+}CD43^{+}IgM^{-}$ B cell precursors. Right, summary of fraction A ($CD24^{-}BP\text{-}1^{-}$), fraction B ($CD24^{+}BP\text{-}1^{-}$), and fraction C/C′ ($CD24^{+}BP\text{-}1^{+}$) cell frequencies. **C** Flow cytometry of GL-7 and Fas expression the Peyer's patches. Right, summary of the GC B cell frequencies. For A-C, WT ($n = 5$), μMT:Cre^{ER}*Rraga*$^{fl/fl}$*Rragb*$^{fl/fl}$ ($n = 6$), and μMT:Cre^{ER}*Rraga*$^{fl/fl}$*Rragb*$^{fl/fl}$*Tfeb*$^{fl/fl}$*Tfe3*$^{-/-}$ ($n = 6$). Splenic B cells were stimulated with LPS/IL-4/BAFF for 72 h. IgG1 expression (**D**), TMRM and MTDR staining (**E**), CellROX staining (**F**), and LAMP1 staining (**G**) were examined by flow cytometry. Summaries of $IgG1^{+}$ B cell frequencies, the relative TMRM, MTDR, CellROX, and LAMP1 MFIs were presented. For (**D**–**G**), $n = 4$ mice for each group. **H** Mitostress assay was performed on a Seahorse XFe96 analyzer. Right, summaries of the basal respiration and maximal respiration. WT ($n = 6$), μMT:Cre^{ER}*Rraga*$^{fl/fl}$*Rragb*$^{fl/fl}$ ($n = 5$), μMT:Cre^{ER}*Rraga*$^{fl/fl}$*Rragb*$^{fl/fl}$*Tfeb*$^{fl/fl}$*Tfe3*$^{-/-}$ ($n = 6$). **I**–**L** Tamoxifen injected WT, μMT:Cre^{ER}*Rraga*$^{fl/fl}$*Rragb*$^{fl/fl}$, and μMT:Cre^{ER}*Rraga*$^{fl/fl}$*Rragb*$^{fl/fl}$*Tfeb*$^{fl/fl}$*Tfe3*$^{-/-}$ chimera mice were immunized intraperitoneally with NP-OVA/alum (**I**, **J**) or TNP-LPS (**K**, **L**). **I** Flow cytometry of CD138 and B220 expression on splenic lymphocytes. Right, summary of $CD138^{+}$ plasmablast frequencies. **J** Flow cytometry of GL-7 and Fas expression on splenic B cells. Right, summary of GC B cell frequencies. For (**I** and **J**), WT ($n = 4$), μMT:Cre^{ER}*Rraga*$^{fl/fl}$*Rragb*$^{fl/fl}$($n = 3$), and μMT:Cre^{ER}*Rraga*$^{fl/fl}$*Rragb*$^{fl/fl}$*Tfeb*$^{fl/fl}$*Tfe3*$^{-/-}$ ($n = 4$). **K** Flow cytometry of CD138 and B220 expression on splenic lymphocytes. Right, summary of $CD138^{+}$ plasmablast frequencies. **L** ELISA measurement of serum TNP-specific antibodies. For (**K** and **L**), WT ($n = 6$), μMT:Cre^{ER}*Rraga*$^{fl/fl}$*Rragb*$^{fl/fl}$ ($n = 7$), μMT:Cre^{ER}*Rraga*$^{fl/fl}$*Rragb*$^{fl/fl}$*Tfeb*$^{fl/fl}$*Tfe3*$^{-/-}$ ($n = 6$). Data in graphs represent mean ± SEM. ns, not significant. $^{*}p < 0.05$, $^{**}p < 0.01$, $^{***}p < 0.001$, and $^{****}p < 0.0001$, one-way ANOVA (**A**, **C**, **D**–**K**), two-way ANOVA (**B** and **L**). Source data are provided as a Source Data file.

marrow cells into lethally irradiated (11 Gy) $CD45.1^{+}$ mice by mixing Cre^{ER}*Rraga*$^{+/+}$*Rragb*$^{+/+}$*Rptor*$^{+/+}$ (WT), *Cre*^{ER}*Rraga*$^{fl/fl}$*Rragb*$^{fl/fl}$, *Cre*^{ER}*Rraga*$^{fl/fl}$*Rragb*$^{fl/fl}$*Tfeb*$^{fl/fl}$, *Cre*^{ER}*Rraga*$^{fl/fl}$*Rragb*$^{fl/fl}$*Tfeb*$^{fl/fl}$*Tfe3*$^{-/-}$ or *Cre*^{ER}*Rptor*$^{fl/fl}$ BM with μMT BM at a ratio of 4:1, followed by reconstitution for at least 2 months. Mice were bred and maintained in a specific pathogen-free facility in the Department of Comparative Medicine of the Mayo Clinic. The mice were euthanized by carbon dioxide according to the approved protocol. All animal protocols (A00003354-18-R23) were approved by the Institutional Animal Care and Use Committees (IACUC) of the Mayo Clinic Rochester.

Cell lines

The retroviral packaging Plat-E cells were a gift from Dr. Hongbo Chi (St. Jude Children's Research Hospital) and from female origin. The cells were cultured in Dulbecco's Modified Eagle Medium (DMEM, Thermo Fisher Scientific) supplemented with 10% fetal bovine serum (FBS) and 2 mM glutamine, 100 U/ml Penicillin, and 100 mg/ml Streptomycin and maintained at 37 °C in 5% CO_2. Puromycin (1 mg/ml) and blasticidin (10 mg/ml) antibiotics were also added into the culture medium to maintain selective pressure and were removed one day before retrovirus plasmid transfection.

Immunizations and other mouse experimentation

For tamoxifen treatment, mice were injected intraperitoneally with tamoxifen (1 mg per mouse) in corn oil daily for four consecutive days and analyzed 7 days after the last injection. For experiments involving an immune challenge, chimeras were given tamoxifen (1 mg per mouse) in corn oil daily for four consecutive days via oral gavage and challenged with antigens or influenza at day 7 after the last tamoxifen administration. For NP-OVA immunization experiments, antigen for immunization was prepared by mixing NP_{23}-OVA (23 molecules of NP linked to OVA; Biosearch Technologies), 10% $KAL(SO_4)_2$ dissolved in PBS at a ratio of 1:1, in the presence of LPS (Escherichia coli strain 055:B5; Sigma) at pH 7. Mice were immunized intraperitoneally (100 μg NP-OVA and 10 μg LPS) for analysis of NP-specific antibody response. Nine days after immunization, sera, spleens, and mesenteric lymph nodes were collected from the mice. Thirteen days after infection, spleens, mediastinal lymph nodes, and lungs from the mice were harvested for analysis. For T-independent immune response, mice were given 50 μg TNP-LPS (Biosearch Technologies) intraperitoneally. Sera and spleens were collected on day 9 after immunization.

Cell isolation and culture

Mouse B cells were isolated from pooled single cell suspensions of spleen and peripheral lymph nodes using CD19 microbeads (Miltenyi, catalog no. 130-052-201) or EasySep Mouse B Cell Isolation Kit (Stemcell Technologies, catalog no. 19854). B cells were cultured in RPMI1640 medium supplemented with 10% (vol/vol) FBS and 1% penicillin-streptomycin and activated with 3 μg/mL LPS (Sigma-Aldrich), 10 ng/mL recombinant mouse IL-4 (Tonbo Bioscience) plus 20 ng/mL recombinant human BAFF (Biolegend) for 3 days. Alternatively, B cells were activated with10 μg/mL anti-IgM (Jackson Immunoresearch), 5 μg/mL anti-CD40 (Bio X Cell) and 10 ng/mL recombinant mouse IL-4, or 2.5 μM CpG ODN2006 (Integrated DNA Technologies) together with 10 ng/mL recombinant mouse IL-4 or 3 μg/mL LPS with 10 ng/mL recombinant murine IFN-γ (Peprotech) and 20 ng/mL recombinant human BAFF or 5 μg/mL anti-CD40 (Bio X Cell) and 10 ng/mL recombinant mouse IL-4. B cell proliferation was measured by CellTrace violet dye dilution (Thermo Fisher Scientific).

Retroviral constructs and transductions

WT TFEB retroviral constructs were made by inserting the cDNA of mouse TFEB isoform b into the MSCV-IRES-EGFP retroviral vector. Ca TFEB retroviral constructs were generated by mutating mouse TFEB isoform b at Ser142 and Ser211 to Ala, and the mutated form was inserted into the MSCV-IRES-EGFP vector. TFEB TDN retroviral construct was generated by deleting activation domain (AD), binding region (BR), and proline-rich region while retaining bHLH and Leucine-zipper region. HA-tag and nuclear location sequence were added at C terminal of the construct. Mito-QC reporter retroviral construct was a gift from Dr. Ping-Chih Ho (Ludwig Institute for Cancer Research), as described previously[57]. To obtain infectious retroviral stocks, each construct was transfected into Plat-E cells along with pCL-Eco packaging plasmid using Lipofectamine™ 3000 Transfection Reagent. Spleen B cells were activated with 3 μg/mL LPS, 10 ng/mL recombinant mouse IL-4, or 0.25 μg/ml anti-CD180 for 40 h, followed by transduction with indicated viruses in the presence of 8 μg/ml polybrene at 32 °C, 1000 × *g* for 90 min. Transduced B cells were put in the 37 °C incubator for 4 h, then changed to fresh medium with 3 μg/mL LPS, 10 ng/mL recombinant mouse IL-4, and 20 ng/mL recombinant human BAFF for further activation. Transduced cells were analyzed after 3 days of activation.

Flow cytometry

For analysis of surface markers, cells were stained in phosphate-buffered saline (PBS) containing 1% (w/v) bovine serum albumin (BSA) with indicated antibodies. The following antibodies were used: anti-B220 (RA3-6B2, 1:300), anti-CD19 (6D5, 1:300), anti-TCRβ (H57-597, 1:300), anti-CD24 (M1/69, 1:1000), anti-BP-1 (6C3, 1:200), anti-IgD (11-26c.2a, 1:400), anti-IgG1 (RMG1-1, 1:200), anti-CD25 (PC61, 1:300), anti-CD4 (RM4-5, 1:300), anti-CD21 (7E9, 1:500), anti-CD23 (B3B4, 1:200), anti-CD93 (AA4.1, 1:300), anti-CD138 (281-2, 1:300), anti-GL7 (GL7, 1:300), anti-CD278 (C398.4A, 1:200), anti-PD-1 (J43, 1:400), anti-CD86 (GL-1, 1:300), anti-IL-7Ra (A7R34, 1:200), and anti-CD71 (R17217, 1:500) were all from Biolegend, anti-IgM (II/41, 1:200) and anti-CD184 (2B11, 1:100) were purchased Thermo Fisher Scientific. Anti-CD95 (Jo2, 1:300), and anti-CD43 (S7, 1:300) were obtained from BD Biosciences. CXCR5 was stained with biotinylated anti-CXCR5 (2G8, 1:100) and

streptavidin-conjugated PE (both from BD Biosciences, 1:200) to enhance the signal. Intracellular Foxp3 (FJK-16s, 1:100), Ki-67 (SolA15, Thermo Fisher Scientific, 1:500), and anti-Bcl6 (K112-91, BD Biosciences, 1:50) were analyzed in cells fixed and permeabilized with Foxp3 staining buffers according to the manufacturer's instructions (Thermo Fisher Scientific). For phosflow staining, cells were stained with surface markers, then fixed with 1× Lyse/Fix (BD Biosciences) buffer at 37 °C for 10 min, washed and permeabilized by ice-cold Perm III buffer (BD Biosciences) on ice for 30 min, followed by staining with anti-phospho-S6 (S235/236, 1:400) or anti-phospho-4E-BP1 (T37/46, 1:200) (both from Cell Signaling Technology) for 30 min at room temperature. Active Caspase-3 was stained according to the manufacturer's instructions (#550914, BD Pharmingen). Briefly, cells were stained with Ghost Dye™ Violet 510 Fixable Viability in PBS at room temperature for 30 min, and the surface markers were stained in FACS buffer on ice for 30 min, then the cells were washed with cold PBS and suspended in BD Cytofix/Cytoperm™ solution at a concentration of 1×10^6 cells/0.5 ml for 20 min, followed by washing with BD Perm/Wash™ buffer at a volume of 0.5 ml buffer/1×10^6 cells at room temperature and stained with active Caspase-3 diluted in BD Perm/Wash™ buffer at room temperature for 30 min. Cell viability was examined by Fixable viability dye (Tonbo Bioscience) or 7-AAD (Thermo Fisher Scientific) following the manufacturer's protocol. For LAMP1 staining, surface staining was done with FACS buffer on ice, followed by fixation and permeabilization using BD Cytofix/Cytoperm Fixation/Permeabilization Kit (BD Biosciences), LAMP1 antibody (1D4B, BioLegend, 1:100) was diluted in BD Perm/Was Buffer and stained at room temperature for 30 min. For the dye staining, B cells were stained with 20 nM MitoTracker Deep Red (ThermoFisher Scientific), 20 nM MitoTracker Green (ThermoFisher Scientific), 100 nM tetramethylrhodamine methyl ester (TMRM, ThermoFisher Scientific). 500 nM CellROX or 1 μM MitoSOX in HBSS at 37 °C for 20 min. Flow cytometry was performed on a BD Fortessa X-20 or LSR II instrument or Attune NxT system (Life Technologies). Data were then analyzed by FlowJo software (Tree Star). Gating strategies were summarized in Supplementary Fig. 8.

p-S65-Ub sandwich ELISA

Levels of phosphorylated ubiquitin at serine 65 (p-S65-Ub) were assessed in a sandwich type ELISA on a Meso Scale Discovery (MSD) platform that uses electrochemiluminescence (ECL) as a readout, which was slightly modified from Watzlawik et al.[68]. In brief, here we used a SULFO-TAG-labeled mouse anti-Ub antibody (clone P4D1) instead of two subsequent detecting antibodies (1. Ub (P4D1) followed by 2. SULFO-TAG-labeled anti-mouse antibody) as described previously[68].

A. *SULFO-TAG-labeling:* For SULFO-TAG-labeling of the Ub detecting antibody (ThermoFisher #14-6078-37, Ub (clone P4D1)), we first removed sodium azide by using Amicon ultra 0.5 ml centrifugal filters with a 50 kDa MWCO (Millipore, UFC505008) and washed 5 times with PBS, pH: 7.9 at 14,000 × g for 2 minutes. Sample recovery was done by inverting the filter in a new tube and spinning for another 2 minutes at 1000 × g. Ub (P4D1) antibody was then incubated at room temperature for 2 h with SULFO-TAG NHS-Ester (MSD, #R31AA) in a challenge ratio of 20:1 (Sulfotag NHS-Ester: antibody) on a rotational shaker. Excess, non-conjugated SULFO-TAG was removed by using a 0.5 ml Zeba Spin desalting column (40 K MWCO) (ThermoFisher, A57760) according to the manufacturer's recommendation.

B. *p-S65-Ub ELISA:* p-S65-Ub antibody (CST #62802) was used as a capture antibody in a concentration of 1 μg/ml in 200 mM sodium carbonate buffer pH 9.7 and coated overnight at 4 °C with 30 μl per well in 96-well MSD plate (MULTI-ARRAY® 96-well Plate; L15XA-3). The next morning MSD plates were washed 2 times with 0.22-micron filtered ELISA wash buffer (150 mM Tris, pH 7.4, 150 mM NaCl, 0.1% [v:v] Tween-20) and subsequently blocked by adding ELISA blocking buffer (150 mM Tris, pH 7.4, 150 mM NaCl, 0.1% [v:v] Tween-20, 1% BSA [w:v]) and incubated for 1 h at 22 °C without shaking. All samples were run in duplicates and diluted in blocking buffer using 10 μg of total protein per well. Antigens were incubated for 2 h at 22 °C on a microplate mixer (USA Scientific, 8182-2019) at 500 rpm and three washing steps were then performed as described before. SULFO-TAG-labeled Ub (P4D1) antibody (1 μg/ml) was added in blocking buffer in 50 μl total volume per well and incubated for 2 h at 22 °C on a microplate mixer at 500 rpm. After three washing steps, 150 μl MSD GOLD Read Buffer (R92TG-2) were finally added to each well and the plate being read on a MESO QuickPlex SQ 120 reader.

Metabolic assays

The bioenergetic activities of B cells, displayed by both ECAR and OCR were measured by Seahorse assays according to the established protocols from Agilent Technologies. Briefly, B cells were seeded at 150, 000-300, 000 cells/well on Cell-Tak (Corning) coated XFe96 plate in indicated medium (For OCR: Seahorse XF RPMI medium containing 10 mM glucose, 2 mM L-glutamine, and 1 mM sodium pyruvate, pH 7.4; For ECAR: Seahorse XF RPMI medium plus 2 mM L-glutamine, pH 7.4; all reagents from Agilent Technologies). For the Mito stress test, OCR and ECAR were measured in the presence of Oligomycin (1.5 μM, Sigma-Aldrich), FCCP (1.5 μM, Sigma-Aldrich), and Rotenone (1 μM, Sigma-Aldrich)/ Antimycin A (1 μM, Sigma-Aldrich). For glycolysis stress, both OCR and ECAR were measured by sequential injection of Glucose (10 mM, Agilent Technologies), Oligomycin (1.5 μM, Sigma-Aldrich), 2-DG (50 mM, Sigma-Aldrich). Glycolytic flux was also measured by detritiation of [3-^{3}H]-glucose (Perkin Elmer) as described[73]. Briefly, 1 μCi [3-^{3}H] glucose was added into the culture media, and 2 h later, 500 μL media were transferred to a 1.5 mL microcentrifuge tube containing 50 μL of 5 N HCl. The microcentrifuge tubes were then placed in 20 mL scintillation vials containing 0.5 ml water with the vials capped and sealed. ^3H_2O was separated from unmetabolized [^{3}H] glucose by evaporative diffusion for 24 h at room temperature. A cell-free sample containing 1 μCi ^{3}H-glucose was included as a background control.

Transmission electron microscopy

B cells were cultured with LPS, IL-4 plus BAFF for 3 days, and cell pellets were harvested and fixed in 2% paraformaldehyde and 2.5% glutaraldehyde in 0.1 M sodium cacodylate. Following fixation, cells were embedded and sliced for transmission electron microscopy. The Grids were imaged with a JEM1400 plus transmission electron microscope (JEOL). Damaged mitochondria with mitophagy were defined as either no visible cristae, surrounded by a phagophore, or being located inside an amphisome.

Single-cell RNA sequencing analysis

The primary data was obtained from ArrayExpress (E-MTAB-9478), followed by annotation and alignment using CellRanger (v3.0.0). All samples from spleen were included. Events with 200-5000 genes detected per cell (nFeature) and <5% mitochondrial genes were put through further analysis with the package of Seurat (v4) in R project. The original code can be found on the official (https://satijalab.org/seurat/articles/integration_introduction.html). In brief, differentially expressed genes were found in each dataset using Principal Component Analysis. Shared genes were then identified across different time points as "anchors" to integrate all datasets. Subsequently, clustering was performed based on K-nearest neighbor (KNN) graph constructed. Clusters resembled contaminating cells (i.e., T cells, myeloid cells, etc.) were excluded. The data was re-clustered using the workflow described previously.

For cell function evaluation, the "AddModuleScore ()" function implanted in Seurat was utilized. Gene sets displayed in Fig. 5L-M included the following: Hallmark mTORC1 signaling (MSigDB, M5924),

Hallmark oxidative phosphorylation (MSigDB, M5936), Putative TFEB target genes (described previously[62]), KEGG Lysosome (MSigDB, M11266), GO lysosome localization (GO:0032418), mitochondrial complex I (MSigDB, M39781), Reactome mitophagy (MSigDB, M27418), and Reactome PINK1-PRKN mediated mitophagy (MSigDB, M27419).

Bulk RNA sequencing

WT or RagA/RagB deficient B cells were activated in vitro for 72 h with LPS, IL-4, and BAFF. RNA was isolated using a Quick-RNA Microprep kit (ZYMO research) following the manufacturer's instructions. After quality control, high-quality total RNA was used to generate the RNA sequencing library. Reads with low quality, containing the adapter (adapter pollution), or with high levels of N base were removed to generate clean data. HISAT(V2.2.1)[74] was used to align the clean reads to the mouse reference genome (*Mus_musculus*, GCF_000001635.27_GRCm39). Bowtie2(V2.4.5)[75] was used to align the clean reads to the reference genes. DEG analysis was carried out using DESeq2[76], and genes with log2FC > 0 and false discovery rate <0.05 were considered for gene cluster analysis.

Nuclear and cytoplasmic extraction

Two million B cells were collected and washed with ice-cold PBS twice, discarded the supernatant, and collected the cell pellets. Gently resuspend cells in 200 µl 1× Hypotonic Buffer (20 mM Tris-HCl, pH 7.4, 10 mM NaCl, 3 mM $MgCl_2$) by pipetting up and down several times, then incubated on ice for 15 min. 15 µl detergent (10% NP40) was added into the suspension and vortexed for 10 s at the highest speed. The supernatant was collected after centrifuging for 10 min at 5000 rpm at 4 °C. This supernatant contains the cytoplasmic fraction. The collected cell pellets were washed once with 1× Hypotonic Buffer and resuspended in 50 µl Complete Cell Extraction Buffer (10 mM Tris, pH 7.4, 2 mM Na_3VO_4, 100 mM NaCl, 1% Triton X-100, 1 mM EDTA, 0% glycerol, 1 mM EGTA, 0.1% SDS, 1 mM NaF, 0.5% deoxycholate, 20 mM $Na_4P_2O_7$) for 30 min on ice with vortexing at 10 min intervals. The supernatant (nuclear fraction) was collected after centrifuging for 30 min at 14,000 × *g* at 4 °C, and the nuclear extracts were ready for assay.

Immunoblots

B cells were lysed in radioimmunoprecipitation assay (RIPA) buffer (50 mM Tris (pH 7.4), 150 mM NaCl, 1% NP-40, 0.5% sodium deoxycholate, 0.1% sodium dodecyl sulfate (SDS)) supplemented with protease inhibitor cocktail and phosphatase inhibitor cocktail (Sigma-Aldrich). Protein concentration was detected by BCA assay (Thermo Fisher Scientific), and an equal amount of protein was resolved in 4–12% SDS-polyacrylamide gel electrophoresis (SDS-PAGE) (Bio-Rad). Proteins were transferred to polyvinylidene difluoride membranes (Millipore) and probed overnight with the following primary antibodies: anti-p-S6K (108D2, 1:1000), anti-p-S6 (D57.2.2E, 1:1000), anti-LAMP1(C54H11, 1:1000), anti-p-4EBP1 (236B4, 1:1000), anti-Raptor (24C12, 1:1000), and anti-RagA (D8B5, 1:1000) all from Cell Signaling Technology), anti-AID (mAID-2, Thermo Fisher Scientific, 1:1000), anti-TFEB (A303-673A, Bethyl Laboratories, 1:1000), Lamin B (66095-1-Ig, Proteintech, 1:5000), tubulin (11224-1-AP, Proteintech, 1:5000), TFE3 (HPA023881, Sigma-Aldrich, 1:1000) and anti-β-actin (13E5, Sigma-Aldrich, 1:5000). The membrane was washed and incubated with indicated secondary antibody for the subsequently enhanced chemiluminescence (ECL, Thermo Fisher) exposure.

Immunofluorescence

For observing the germinal center structure in the spleen, part of the spleen from the immunized or infected mice was fixed in 4% Paraformaldehyde at 4 °C overnight, then the spleens were dehydrated in 20% sucrose for at least 36 h. Then the spleens were embedded in OCT and sectioned at 5 µm thickness. The slides were air-dried at room temperature before being fixed in cold acetone at −20 °C for 10 min. The fixed slides were washed with PBS for twice and blocked with Blocking buffer (Thermo Fisher Scientific) for 1 h at room temperature. Biotinylated Peanut Agglutinin (PNA, Vector laboratories, 1:1000) was stained on the sections at 4 °C overnight. The slides were washed with PBST 3 times, then the Alexa Fluor™ 488 Conjugated Streptavidin (1:1000), anti-mouse CD21/CD35 (Alexa Fluor® 594, Biolegend, 1:200), and anti-mouse IgD (Alexa Fluor® 647 anti-mouse IgD, Biolegend, 1:100) was applied onto the section for 2 h at room temperature. After washing with PBST for 3 times, the slides were counterstained with 4', 6-diaminodino-2-phenylindole (DAPI) and mounted. The stained slides were reviewed, and representative images were acquired on Olympus DP80 digital microscope.

RNA isolation and real-time quantitative PCR

Total RNA was extracted using the RNeasy Micro kit (Qiagen) according to the manufacturer's instructions, and total RNA was reverse transcribed into cDNA by PrimeScript RT Reagent Kit (Takara) following the established protocol of the kit. The mRNA level of *Rragd, Rragc, Bhlhe40*, and *Prodh2* was detected by real-time PCR with a Thermo Fisher Real-time PCR system, while β-actin was used as an internal control. Each sample was analyzed in triplicate and the relative amount of gene expression was calculated using the $2^{-\Delta\Delta Ct}$ method. Primer sequences were summarized in Supplementary Table.

ELISA

For detecting NP-specific antibodies in sera, wells were coated with 1 µg/mL NP_{23}-BSA or NP_2-BSA in coating buffer (Bicarbonate-carbonate buffer, pH 9.6) overnight. Plates were washed twice with washing buffer (0.05% Tween 20 in PBS), blocked with 5% blocking protein (Bio-Rad) at 37 °C for 1 h, washed twice, and incubated with indicated sera samples at 37 °C for 1.5 h. Horseradish peroxidase (HRP)-conjugated secondary antibodies: anti-mouse IgG1, anti-mouse IgG2b, anti-mouse IgG2c, and anti-mouse IgG3 (all from SouthernBiotech), or anti-mouse IgM (Bethyl laboratories) were developed at 37 °C for 1 h after washing with a buffer for four times. The reaction was further developed with tetramethylbenzidine (TMB), then stopped by 2 N H_2SO_4, and read at 450 nm.

Preparation of amino acid medium

Amino acid-free (AA-) medium was prepared by RPMI 1640 powder (R8999-04A, US Biological Life Science) and sodium phosphate dibasic (5.6 mM, the same concentration as commercially available RPMI 1640 medium, US Biological Life Science), supplemented with 10% (v/v) dialyzed FBS (Thermo Fisher Scientific). Amino acid-sufficient (AA +) medium was prepared by adding proper volumes of MEM amino acids solution (essential amino acids, EAA, 50×), MEM non-essential amino acids solution (NEAA, 100×), and 200 mM L-Gln (all from Sigma-Aldrich) to AA- medium to reach a final concentration of 1×EAA, 1×NEAA, and 2 mM Gln. The medium was supplemented with 10% (v/v) dialyzed FBS. Medium containing single amino acids (Ala, Leu, Gln, or Arg) or their combinations was prepared with AA− medium (prepared to the same concentrations present in the AA+ medium). All media were adjusted to pH7.5 and filter-sterilized (0.2 µm) before use.

Statistical analysis

Statistics were performed on GraphPad Prism 8. P values were calculated with Student's *t*-test, one-way ANOVA, or two-way ANOVA, as indicated in the figure legends. $p < 0.05$ was considered significant. All error bars were represented as SEM.

Reporting summary

Further information on research design is available in the Nature Portfolio Reporting Summary linked to this article.

Data availability

Source data are provided with this paper and can be accessed at https://figshare.com/s/b5b8e00a13fba9db6caa. Sequencing data have been deposited in Sequence Read Archive and can be accessed at https://www.ncbi.nlm.nih.gov/bioproject?term=PRJNA1093059&cmd=DetailsSearch Source data are provided with this paper.

References

1. Rawlings, D. J., Schwartz, M. A., Jackson, S. W. & Meyer-Bahlburg, A. Integration of B cell responses through Toll-like receptors and antigen receptors. *Nat. Rev. Immunol.* **12**, 282–294 (2012).
2. Fagarasan, S. & Honjo, T. T-Independent immune response: new aspects of B cell biology. *Science* **290**, 89–92 (2000).
3. Allman, D., Wilmore, J. R. & Gaudette, B. T. The continuing story of T-cell independent antibodies. *Immunol. Rev.* **288**, 128–135 (2019).
4. Allen, C. D., Okada, T. & Cyster, J. G. Germinal-center organization and cellular dynamics. *Immunity* **27**, 190–202 (2007).
5. Lu, L. L., Suscovich, T. J., Fortune, S. M. & Alter, G. Beyond binding: antibody effector functions in infectious diseases. *Nat. Rev. Immunol.* **18**, 46–61 (2018).
6. Boothby, M. & Rickert, R. C. Metabolic regulation of the immune humoral response. *Immunity* **46**, 743–755 (2017).
7. Jellusova, J. et al. Gsk3 is a metabolic checkpoint regulator in B cells. *Nat. Immunol.* **18**, 303–312 (2017).
8. Zeng, H. et al. Discrete roles and bifurcation of PTEN signaling and mTORC1-mediated anabolic metabolism underlie IL-7-driven B lymphopoiesis. *Sci. Adv.* **4**, eaar5701 (2018).
9. Caro-Maldonado, A. et al. Metabolic reprogramming is required for antibody production that is suppressed in anergic but exaggerated in chronically BAFF-exposed B cells. *J. Immunol.* **192**, 3626–3636 (2014).
10. Sharma, R. et al. Distinct metabolic requirements regulate B cell activation and germinal center responses. *Nat. Immunol.* **24**, 1358–1369 (2023).
11. Xiao, G. et al. B-cell-specific diversion of glucose carbon utilization reveals a unique vulnerability in B cell malignancies. *Cell* **173**, 470–484.e418 (2018).
12. Akkaya, M. et al. Second signals rescue B cells from activation-induced mitochondrial dysfunction and death. *Nat. Immunol.* **19**, 871–884 (2018).
13. Waters, L. R., Ahsan, F. M., Wolf, D. M., Shirihai, O. & Teitell, M. A. Initial B cell activation induces metabolic reprogramming and mitochondrial remodeling. *iScience* **5**, 99–109 (2018).
14. Urbanczyk, S., et al. Mitochondrial respiration in B lymphocytes is essential for humoral immunity by controlling the flux of the TCA cycle. *Cell Rep.* **39**, 110912 (2022).
15. Yazicioglu, Y. F. et al. Dynamic mitochondrial transcription and translation in B cells control germinal center entry and lymphomagenesis. *Nat. Immunol.* **24**, 991 (2023).
16. Raybuck, A. L. et al. mTORC1 as a cell-intrinsic rheostat that shapes development, preimmune repertoire, and function of B lymphocytes. *FASEB J.* **33**, 13202–13215 (2019).
17. Boothby, M. R., Brookens, S. K., Raybuck, A. L. & Cho, S. H. Supplying the trip to antibody production-nutrients, signaling, and the programming of cellular metabolism in the mature B lineage. *Cell Mol. Immunol.* **19**, 352–369 (2022).
18. Kedia-Mehta, N. & Finlay, D. K. Competition for nutrients and its role in controlling immune responses. *Nat. Commun.* **10**, 2123 (2019).
19. DeBoer, M. D. et al. Systemic inflammation, growth factors, and linear growth in the setting of infection and malnutrition. *Nutrition* **33**, 248–253 (2017).
20. Ibrahim, M. K., Zambruni, M., Melby, C. L. & Melby, P. C. Impact of childhood malnutrition on host defense and infection. *Clin. Microbiol Rev.* **30**, 919–971 (2017).
21. Sancak, Y. et al. The Rag GTPases bind raptor and mediate amino acid signaling to mTORC1. *Science* **320**, 1496–1501 (2008).
22. Lawrence, R. E. et al. Structural mechanism of a Rag GTPase activation checkpoint by the lysosomal folliculin complex. *Science* **366**, 971 (2019).
23. Kim, E., Goraksha-Hicks, P., Li, L., Neufeld, T. P. & Guan, K. L. Regulation of TORC1 by Rag GTPases in nutrient response. *Nat. Cell Biol.* **10**, 935–945 (2008).
24. Ortega-Molina, A. et al. Oncogenic Rag GTPase signaling enhances B cell activation and drives follicular lymphoma sensitive to pharmacological inhibition of mTOR. *Nat. Metab.* **1**, 775–789 (2019).
25. Ersching, J. et al. Germinal center selection and affinity maturation require dynamic regulation of mTORC1 kinase. *Immunity* **46**, 1045 (2017).
26. Kalaitzidis, D. et al. Amino acid-insensitive mTORC1 regulation enables nutritional stress resilience in hematopoietic stem cells. *J. Clin. Investig.* **127**, 1405–1413 (2017).
27. Kim, Y. C. et al. Rag GTPases are cardioprotective by regulating lysosomal function. *Nat. Commun.* **5**, 4241 (2014).
28. Shen, K., Sidik, H. & Talbot, W. S. The rag-ragulator complex regulates lysosome function and phagocytic flux in microglia. *Cell Rep.* **14**, 547–559 (2016).
29. Efeyan, A. et al. RagA, but not RagB, is essential for embryonic development and adult mice. *Dev. Cell* **29**, 321–329 (2014).
30. Jewell, J. L. et al. Differential regulation of mTORC1 by leucine and glutamine. *Science* **347**, 194–198 (2015).
31. Zhang, X. et al. Reprogramming tumour-associated macrophages to outcompete cancer cells. *Nature* **619**, 616–623 (2023).
32. Shi, H. et al. Amino acids license kinase mTORC1 activity and Treg cell function via small G proteins rag and Rheb. *Immunity* **51**, 1012–1027.e1017 (2019).
33. Do, M. H., et al. Nutrient mTORC1 signaling underpins regulatory T cell control of immune tolerance. *J. Exp. Med.* **217**, e20190848 (2020).
34. Zeng, H. et al. mTORC1 couples immune signals and metabolic programming to establish T(reg)-cell function. *Nature* **499**, 485–490 (2013).
35. Napolitano, G. & Ballabio, A. TFEB at a glance. *J. Cell Sci.* **129**, 2475–2481 (2016).
36. Martina, J. A., et al. The nutrient-responsive transcription factor TFE3 promotes autophagy, lysosomal biogenesis, and clearance of cellular debris. *Sci. Signal* **7**, ra9 (2014).
37. Settembre, C. et al. TFEB links autophagy to lysosomal biogenesis. *Science* **332**, 1429–1433 (2011).
38. Sardiello, M. et al. A gene network regulating lysosomal biogenesis and function. *Science* **325**, 473–477 (2009).
39. Martina, J. A., Chen, Y., Gucek, M. & Puertollano, R. MTORC1 functions as a transcriptional regulator of autophagy by preventing nuclear transport of TFEB. *Autophagy* **8**, 903–914 (2012).
40. Liu, G. Y. & Sabatini, D. M. mTOR at the nexus of nutrition, growth, ageing and disease. *Nat. Rev. Mol. Cell Bio* **21**, 183–203 (2020).
41. Puertollano, R., Ferguson, S. M., Brugarolas, J., Ballabio, A. The complex relationship between TFEB transcription factor phosphorylation and subcellular localization. *Embo J.* **37**, e98804 (2018).
42. Napolitano, G. et al. A substrate-specific mTORC1 pathway underlies Birt-Hogg-Dube syndrome. *Nature* **585**, 597 (2020).
43. Pastore, N. et al. TFEB and TFE3 cooperate in the regulation of the innate immune response in activated macrophages. *Autophagy* **12**, 1240–1258 (2016).
44. Brady, O. A., Martina, J. A. & Puertollano, R. Emerging roles for TFEB in the immune response and inflammation. *Autophagy* **14**, 181–189 (2018).
45. Huan, C. et al. Transcription factors TFE3 and TFEB are critical for CD40 ligand expression and thymus-dependent humoral immunity. *Nat. Immunol.* **7**, 1082–1091 (2006).

46. Zhang, H. et al. Polyamines control eIF5A hypusination, TFEB translation, and autophagy to reverse B cell senescence. *Mol. Cell* **76**, 110–125.e119 (2019).
47. Xia, M. H., et al. Transcription factor EB coordinates environmental cues to regulate T regulatory cells' mitochondrial fitness and function. *Proc. Natl Acad. Sci. USA* **119**, e2205469119 (2022).
48. Jones, D. D. et al. mTOR has distinct functions in generating versus sustaining humoral immunity. *J. Clin. Investig.* **126**, 4250–4261 (2016).
49. Iwata, T. N. et al. Conditional disruption of raptor reveals an essential role for mTORC1 in B cell development, survival, and metabolism. *J. Immunol.* **197**, 2250–2260 (2016).
50. Ma, Q., Jones, D. & Springer, T. A. The chemokine receptor CXCR4 is required for the retention of B lineage and granulocytic precursors within the bone marrow microenvironment. *Immunity* **10**, 463–471 (1999).
51. Zhao, R. et al. A GPR174-CCL21 module imparts sexual dimorphism to humoral immunity. *Nature* **577**, 416–420 (2020).
52. Kara, E. E. et al. Atypical chemokine receptor 4 shapes activated B cell fate. *J. Exp. Med.* **215**, 801–813 (2018).
53. Basso, K. & Dalla-Favera, R. Roles of BCL6 in normal and transformed germinal center B cells. *Immunol. Rev.* **247**, 172–183 (2012).
54. Victora, G. D. & Nussenzweig, M. C. Germinal centers. *Annu. Rev. Immunol.* **40**, 413–442 (2022).
55. Luo, W. et al. SREBP signaling is essential for effective B cell responses. *Nat. Immunol.* **24**, 337 (2023).
56. Akkaya, M. & Pierce, S. K. From zero to sixty and back to zero again: the metabolic life of B cells. *Curr. Opin. Immunol.* **57**, 1–7 (2019).
57. Yu, Y. R. et al. Disturbed mitochondrial dynamics in CD8(+) TILs reinforce T cell exhaustion. *Nat. Immunol.* **21**, 1540–1551 (2020).
58. Scharping, N. E. et al. The tumor microenvironment represses T cell mitochondrial biogenesis to drive intratumoral T cell metabolic insufficiency and dysfunction. *Immunity* **45**, 701–703 (2016).
59. Cunningham, J. T. et al. mTOR controls mitochondrial oxidative function through a YY1-PGC-1α transcriptional complex. *Nature* **450**, 736–U712 (2007).
60. Morita, M. et al. mTORC1 controls mitochondrial activity and biogenesis through 4E-BP-dependent translational regulation. *Cell Metab.* **18**, 698–711 (2013).
61. Larsson, N. G. et al. Mitochondrial transcription factor A is necessary for mtDNA maintenance and embryogenesis in mice. *Nat. Genet* **18**, 231–236 (1998).
62. Guo, C. S. et al. SLC38A2 and glutamine signalling in cDC1s dictate anti-tumour immunity. *Nature* **620**, 200 (2023).
63. Wang, S. J. et al. Emerging role of transcription factor EB in mitochondrial quality control. *Biomed. Pharmacother.* **128**, 110272 (2020).
64. Cui, M. et al. HKDC1, a target of TFEB, is essential to maintain both mitochondrial and lysosomal homeostasis, preventing cellular senescence. *Proc. Natl Acad. Sci. USA* **121**, e2306454120 (2024).
65. McWilliams, T. G. et al. mito-QC illuminates mitophagy and mitochondrial architecture in vivo. *J. Cell Biol.* **214**, 333–345 (2016).
66. Young, N. P. et al. AMPK governs lineage specification through Tfeb-dependent regulation of lysosomes. *Gene Dev.* **30**, 535–552 (2016).
67. Song, J. X. et al. A novel curcumin analog binds to and activates TFEB in vitro and in vivo independent of MTOR inhibition. *Autophagy* **12**, 1372–1389 (2016).
68. Watzlawik, J. O. et al. Sensitive ELISA-based detection method for the mitophagy marker p-S65-Ub in human cells, autopsy brain, and blood samples. *Autophagy* **17**, 2613–2628 (2021).
69. Bourke, C. D., Berkley, J. A. & Prendergast, A. J. Immune dysfunction as a cause and consequence of malnutrition. *Trends Immunol.* **37**, 386–398 (2016).
70. Goberdhan, D. C., Wilson, C. & Harris, A. L. Amino acid sensing by mTORC1: intracellular transporters mark the spot. *Cell Metab.* **23**, 580–589 (2016).
71. Price, M. J., Patterson, D. G., Scharer, C. D. & Boss, J. M. Progressive upregulation of oxidative metabolism facilitates plasmablast differentiation to a T-independent antigen. *Cell Rep.* **23**, 3152–3159 (2018).
72. Settembre, C. et al. TFEB controls cellular lipid metabolism through a starvation-induced autoregulatory loop. *Nat. Cell Biol.* **15**, 1016–1016 (2013).
73. Zeng, H. et al. mTORC1 and mTORC2 kinase signaling and glucose metabolism drive follicular helper T cell differentiation. *Immunity* **45**, 540–554 (2016).
74. Kim, D., Langmead, B. & Salzberg, S. L. HISAT: a fast spliced aligner with low memory requirements. *Nat. Methods* **12**, 357–360 (2015).
75. Langmead, B. & Salzberg, S. L. Fast gapped-read alignment with Bowtie 2. *Nat. Methods* **9**, 357–359 (2012).
76. Love, M. I., Huber, W. & Anders, S. Moderated estimation of fold change and dispersion for RNA-seq data with DESeq2. *Genome Biol.* **15**, 550 (2014).

Acknowledgements

We thank Drs. Hongbo Chi, Andrea Ballabio, Ming O. Li, Ping-Chih Ho, Christopher AJ. Roman for sharing mouse strains and research reagents. We acknowledge the Microscopy and Cell Analysis Core at Mayo Clinic Rochester. We acknowledge the NIH (grants R01 AI 162678 and R01 AR077518) for supporting this work in H.Z.'s laboratory, and R01 AI154598, R01 AI147394, R01 AI176171 and R01 AI 112844 to J.S.'s laboratory.

Author contributions

X.X.Z. and H.Z. conceived the project, designed the research, interpreted the data, and wrote the manuscript. X.X.Z. and X.Z. prepared the materials and carried out the experiments. Y.W. and Y.M.C. performed the bioinformatics analysis. Y.L. managed the mouse colony, performed molecular biology experiments and fluorescence imaging. D.D.B. provided imaging analysis. V.S.S. provided antibodies and other research materials. J.O.W. and W.S. performed part of the mitophagy analyses. A.L.R. provided tissue samples from Raptor mutant mouse line. M.R.B. interpreted the data and revised the manuscript. This work is a collaboration with J.S. and M.R.B., who provided key materials and expertize for the research.

Competing interests

The authors declare no competing interests.

Additional information

Supplementary information The online version contains supplementary material available at https://doi.org/10.1038/s41467-024-54344-5.

Correspondence and requests for materials should be addressed to Hu Zeng.

Peer review information *Nature Communications* thanks Hassan Jumaa and the other, anonymous, reviewer(s) for their contribution to the peer review of this work. A peer review file is available.

Reprints and permissions information is available at http://www.nature.com/reprints

Publisher's note Springer Nature remains neutral with regard to jurisdictional claims in published maps and institutional affiliations.

Open Access This article is licensed under a Creative Commons Attribution-NonCommercial-NoDerivatives 4.0 International License, which permits any non-commercial use, sharing, distribution and reproduction in any medium or format, as long as you give appropriate credit to the original author(s) and the source, provide a link to the Creative Commons licence, and indicate if you modified the licensed material. You do not have permission under this licence to share adapted material derived from this article or parts of it. The images or other third party material in this article are included in the article's Creative Commons licence, unless indicated otherwise in a credit line to the material. If material is not included in the article's Creative Commons licence and your intended use is not permitted by statutory regulation or exceeds the permitted use, you will need to obtain permission directly from the copyright holder. To view a copy of this licence, visit http://creativecommons.org/licenses/by-nc-nd/4.0/.

© The Author(s) 2024